Concord McNair Scholars Research Journal

Volume 16 (2013)

Table of Contents

Characterization of a mylonite dike containing pseudotachylyte from the Homestake Shear Zone in Colorado, USA

Christina Facemyer

Abstract

A mafic dike containing pseudotachylyte located in the Homestake shear zone in Colorado was studied. The pseudotachylyte and the dike hosting it are chemically similar, and the pseudotachylyte contains inclusions from the host rock. The pseudotachylyte is interpreted to once have been pristine pseudotachylyte that was then overprinted by metamorphism making up the rest of the dike. The pseudotachylyte is localized by the lithology of the dike, unlike other pseudotachylytes in the Homestake shear zone which are localized by the fabric of the host rock.

Introduction

Pseudotachylyte is a black-gray aphantic rock that looks like black basaltic glass (tachylyte). It occurs as thin veins, injection veins, and sometimes as a matrix to pseudo-conglomerates and breccias (Bucher and Frey, 1994). It is sometimes found in actively deforming mylonitic shear zones, as a result of high pressure rupturing. Most pseudotachylytes appear to have been formed in or near the upper crustal seismogenic zone; however in subduction zones pseudotachylyte may develop much deeper (40-60 km) (Sibson and Toy, 2006).

In thin section, pseudotachylyte appears as a light brown to black fine-grained matrix. Clasts from the host rock may be found in this matrix. Clasts commonly found in pseudotachylyte are monocrystalline and polycrystalline quartz with small amounts of plagioclase and alkali feldspar (Maddock and Grocott, 1987). Clasts of magnetite, zircon, allanite, biotite, and hornblende are usually present, but much less abundant (Allen and Shaw, 2011).

It can be difficult to distinguish genuine pseudotachylyte from similar rocks. Dark, fine- grained rocks described as pseudotachylyte in the field may actually be ultracataclasite or ultramylonite

(Sibson and Toy, 2006). The similarity of these rocks makes them difficult to distinguish in hand sample and thin section. Optical and electron microscopy are needed to confirm a rock as genuine pseudotachylyte. Flow textures, chill margins, preserved quench textures with sperulites in the groundmass, and dominance of angular quartz clasts over rounded feldspar are evidence of pseudotachylyte found using microscopy (Sibson and Toy, 2006).

Mylonite is a fine grained, foliated metamorphic rock. Mylonites are characterized by lineation and distinctive foliation; they typically occur in shear zones that range from millimeters to hundreds of meters in width. They are produced by dynamic recrystallization (nucleation and growth of new grains occurs during deformation as opposed to afterwards as in static recrystallization) and ductile deformation of minerals. These rocks form in fault shear zones at a depth where crystal-plastic deformation is dominant (10-15 km within the crust). Mylonites may or may not contain porphyroclasts (Lin, 2008). The proportions of porphyroclasts to matrix are used to subdivide mylonites into protomylonite (10-50% matrix), mylonite (50-90%), and ultramylonite (greater than 90% matrix) (Lin, 2008). A rock is mylonitic if it shows evidence of reduction in grain size, foliation associated with crystal-plastic deformation and dynamic recrystallization, and occurrence in a planar shear zone (Lin, 2008).

The purpose of this study is to characterize a unique exposure of a mafic dike containing pseudotachylyte; the mafic dike is hosted in gneiss. The objectives are to determine what type of rock the dike was before deformation and metamorphism, determine the current type of rock the dike is, and to determine whether the pseudotachylyte found in the dike is genuine or not.

Geologic Setting

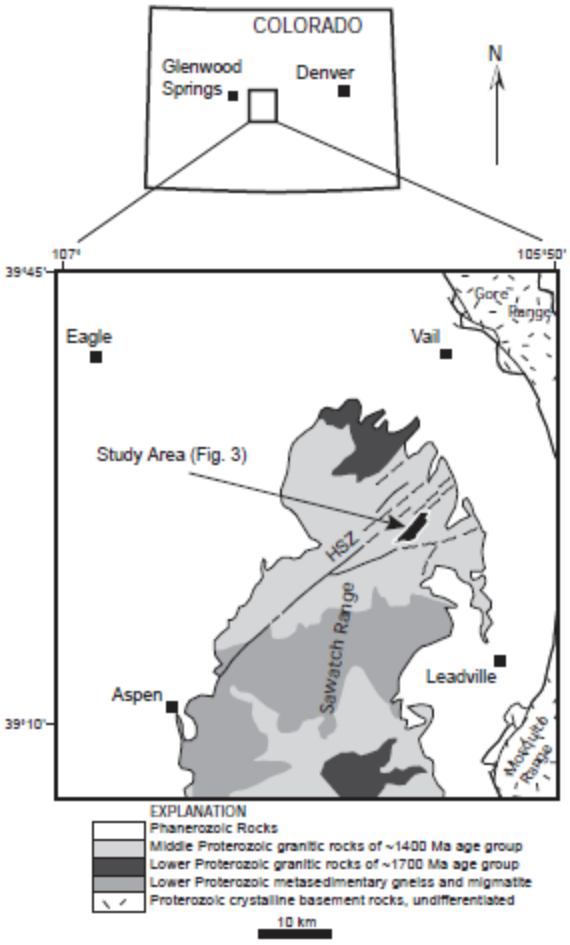

Figure 1: Location of the field area (Allen, 2005). (HSZ=Homestake shear zone)

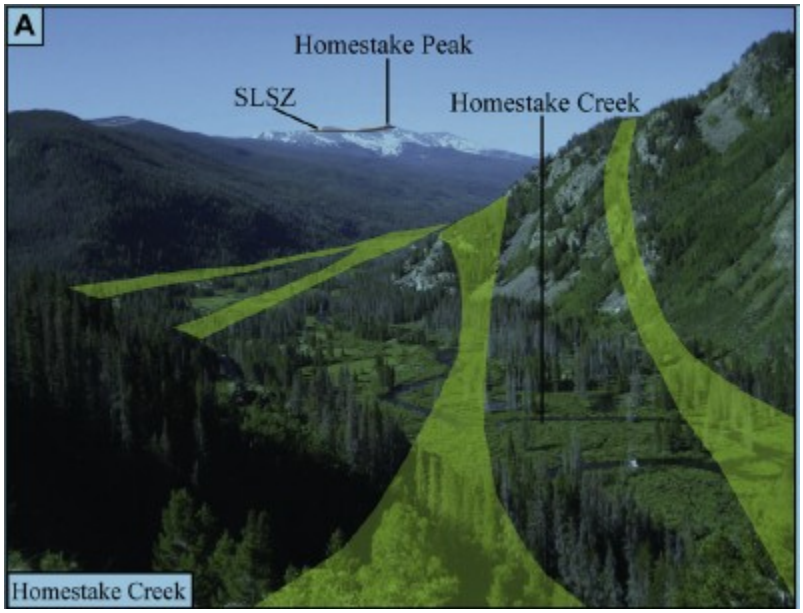

Figure 2: Shaded areas represent the Homestake shear zone, seen from Hornsilver campground. (Lee et al., 2012)

The pseudotachylyte and host-rock samples for this study were taken from the Homestake shear zone in the northeastern Sawatch Range of Colorado, USA (Figures 1 and 2). The Homestake shear zone is a belt of dispersed, individual shear zones about 9 to 11 km wide (Tweto and Sims, 1963). The shear zones are mainly northeast striking and subvertical, and hosted in Proterozoic gneisses and lower to middle Proterozoic plutonic rocks of granite composition (Tweto and Sims, 1963). The exposed rocks of this system are mainly of Precambrian age and are exposed in a system of three branches (Allen, 2005). The dispersed, individual shear zones are usually on the scale of tens of meters wide. Outcrops in these shear zones contain mylonite, ultramylonite, pseudotachylyte, breccia, and a variety of other fault rocks (Allen, 2005). In

general, the pseudotachylyte veins are exposed within northeast-striking fault zones that are exposed about 7.3 km along their strike. The pseudotachylyte in the area is exposed in the form of fault veins of varying thickness (~1mm to 10cm) and injection veins branching off the fault veins at moderate to high angles (Allen, 2005).

The Homestake shear zone is a part of the Proterozoic continental lithosphere of southwestern North America. It assembled about 1.7 Ga and was reactivated about 1.4 Ga during intracontinental transpression (Shaw et al., 2001; Allen, 2005). A quartz-rich, semi-pelitic gneiss, the basement rock unit in the area, hosts most of the Homestake shear zone. The basement is course grained, schist-like, and rich in biotite (Allen, 2005).

During the development of the Homestake shear zone in the Proterozoic, the area is interpreted to have undergone four distinct ductile deformation episodes (Shaw et al., 2001). During a deformation episode of high temperature metamorphism at about 1710 to 1630 Ma, the primary gneissic foliation was isoclinically folded, generating centimeter-to meter-scale granitic dikes, parallel to overprinting asymmetric fold axis (Allen, 2005). In the next event, high-temperature deformation progressed. Foliation, due to crustal shortening, was transposed in a sub-vertical orientation along northeast striking, high strain zone. Around about 1372 Ma these fabrics were over printed by northeast striking, west side up zones of mylonite. Younger zones of mylonite, northwest side down, are associated with crosscutting and ductily sheared pseudotachylyte (the 3rd and 4th deformation events) (Shaw et al, 2001).

Geochemistry and Petrography of Pseudotachylyte and Host Dike

X-ray fluorescence was used to analyze bulk samples of the pseudotachylyte and the mafic-intermediate dike that hosts the pseudotachylyte. Samples were prepared at Concord University by carefully separating pseudotachylyte from the dike using a saw, and then analyzed at Washington State University. Whole rock analysis of samples show the dike contains 57.42%

SiO_2, 15.96% Al_2O_3, 7.77% FeO, 4.72% MgO, 4.98% CaO, and 0.742% P_2O_5. It contains notably high concentrations of K_2O (4.13%), and TiO_2 (1.267%), while its Na_2O content is low, 0.42%.

The composition of the pseudotachylyte is 55.82% SiO_2, 16.18% Al_2O_3, 8.37% FeO, 4.21% MgO, 6.16% CaO, and 1.110% P_2O_5. It is enriched in TiO_2 (1.214%) and K_2O (3.73%), while it has a low Na_2O concentration (0.58%). The composition of the host dike is therefore effectively identical to the pseudotachylyte. The pseudotachylyte and the dike also contain similar concentrations of trace elements, with both rocks enriched in Ba (3755 ppm) and Sr (1441 ppm). Small differences in composition can be attributed to bias in the samples analyzed or statistically insignificant analytical error.

Compared to other host rocks and pseudotachylyte samples taken from the Homestake shear zone, the dike contains significantly less SiO_2. Other samples contain 63.37% to 79.39% SiO_2, while the dike contains 57.42% SiO_2. Also significant is the relatively high concentration of Ti, Ca, P, and K in the dike, while there was a significant decrease in Na.

Figure 3: Mylonite dike with a vein of pseudotachylyte running through the middle.

The host dike forms a sharp contact with the veins of pseudotachylyte. Injection veins can be seen protruding off the fault veins of pseudotachylyte (fig 3). The pseudotachylyte is fine grained, rough-weathering, greyish in color, and contains 1-2mm sized felsic inclusions. Both the pseudotachylyte and dike contain similar mineral content with large amounts of biotite and plagioclase (fig 4a and 4b). The plagioclase and biotite in both is subhedral to euhedral, and it is finer-grained in the pseudotachylyte where it forms the prominent, rough-weathering matrix.

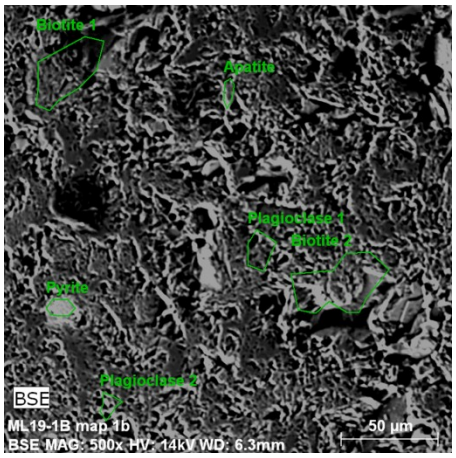

Figure 4a: Pseudotachylyte matrix

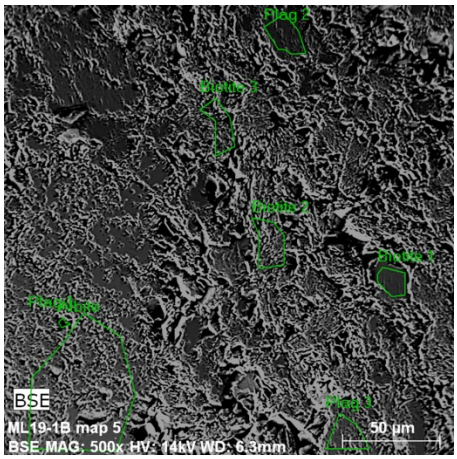

Figure 4b: Host mylonite

Localization of pseudotachylyte

The pseudotachylyte is localized in a mafic dike hosted by gneiss in the Homestake shear zone that is about 1 m wide and around 100 meters long (fig 6). This extreme localization of seismic activity in such a narrow dike is unusual for the Homestake shear zone and has not been reported elsewhere in the literature. Typical localization of pseudotachylyte in the area is fabric controlled. For example, pseudotachylyte found at Hornsilver ridge follows a northeast (060°) trend. Composite fabric in the area follows a 055° to 066° northeastern trend, dipping to the northwest (Shaw et al., 2001). The cross section below shows the fabric orientation at Hornsilver ridge (fig 5); pseudotachylyte has been found to overprint the boundary between S1 and S2 foliation domains (Unpublished field data, 2013 CU Geology Field Camp).

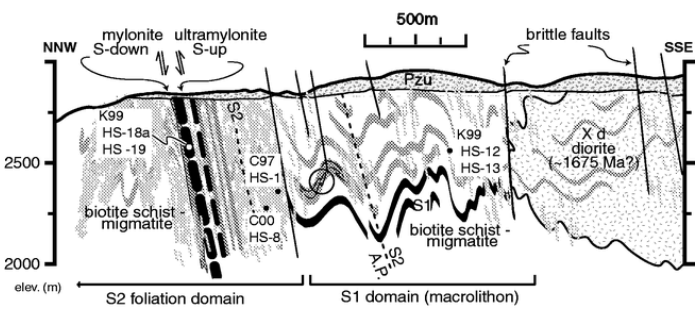

Figure 5: Orientation of fabric at Hornsilver ridge (Shaw et al., 2001).

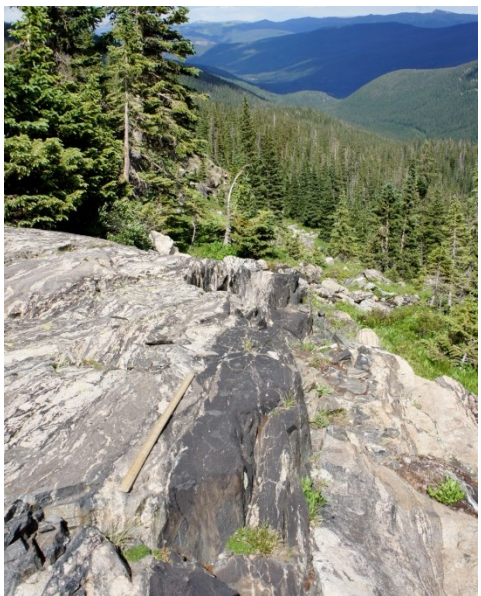

Figure 6: Mafic dike hosted by gneiss

Discussion

Pristine pseudotachylytes are easily lost due to their vulnerability to deformation, alteration, and overprinting. Their fine grain size makes them weaker than surrounding rock which favors localization of ductile flow along the pseudotachylyte, making them susceptible to destruction. There are many processes by which a genuine pseudotachylyte may be destroyed (fig 7), but recognizing pseudotachylyte, even if subsequently changed, is important for estimating how common their occurrence is. Recognizing them is also important for determining the frequency of frictional melt generation during seismic processes (Kirkpatrick and Rowe, 2013). The rate at which they're produced may be underestimated, not only due to difficultly recognizing pseudotachylyte in the field, but also due to how easily they are destroyed (Scholz, 1990).

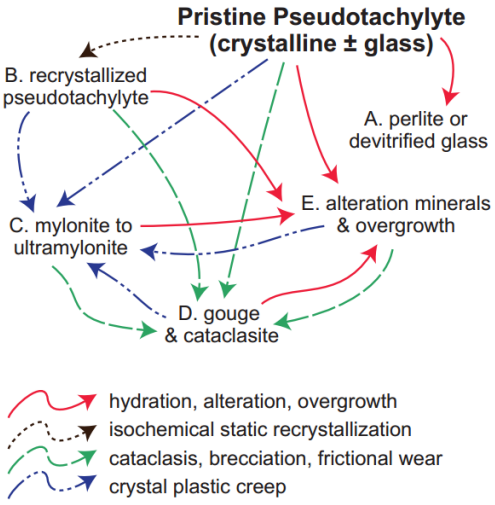

Figure 7: Processes that destroy pseudotachylyte and their outcomes (Kirkpatrick and Rowe, 2013).

The form of the veins hosted in the dike, and the presence of lithic clasts suspended in a finer mineral matrix (now composed of recrystallized biotite) suggests it is pseudotachylyte. In addition, the vein forms a sharp, dark, fine grained, almost glassy contact with the host. Biotite, plagioclase, and other minerals found in the dike are primarily euhedral in shape. Following the

criteria for recognition of reworked pseudotachylyte defined by Kirkpatrick and Rowe (2013), these factors combine to suggest the vein was originally a melt-origin pseudotachylyte. The felsic inclusions in the pseudotachylyte veins are interpreted to be derived from silicic partial melt (leucosomes) present the host dike. The same silicic leucosomes are present in the gneiss that hosts the dike, indicating that both the gneiss and the dike were subject to partial melting prior to generation of the pseudotachylyte. The similar chemistry between the pseudotachylyte and dike, as well as the biotite-rich mineralogy in both the pseudotachylyte and host indicate that the pseudotachylyte in the dike was recrystallized along with the dike. The pseudotachylyte recrystallization occurred under the same pressure and temperature conditions as the host rock, resulting in an equilibrium assemblage of minerals in the dike by static recrystallization (similar processes are described from other locations by Kirkpatrick and Rowe, 2013).

The presence of pseudotachylyte in a 0.5- to 1-meter- wide dike shows that pseudotachylyte can be localized by lithology as well as by fabric. I interpret brittle rupture to have been localized in the dike due to differences in lithology of the mafic dike and its gneiss host, as well as along-strike continuity of the dike. In this interpretation, the sharp contrast between the gneiss host and the mafic dike material may have provided a weak spot making the dike more susceptible to brittle rupture. The relative weakness of the dike compared to the surrounding gneiss favors localization. The long length of the dike further increases the likelihood of localization of brittle fracture.

Conclusions

The pseudotachylyte found in the mafic dike is interpreted to have once been pristine pseudotachylyte due to the vein-form geometry and the presence of relict lithic clasts of leucosomes that are also present in the host dike. Chemical and mineralogic similarities between the pseudotachylyte and the host dike suggest that the pseudotachylyte was recrystallized under

the same conditions that formed the metamorphosed host. The coincidence between the pseudotachylyte and the dike is interpreted to indicate that pseudotachylyte can be localized by lithology as well as by the fabric of the host rock.

References

Allen, J.L., 2005, A multi-kilometer pseudotachylyte system as an exhumed record of earthquake rupture geometry at hypocentral depths (Colorado, USA): Tectonophysics, v. 402, p.37-54

Allen, J.L., O'Hara, K.D., Moecher, D.P., Structural geometry and thermal history of pseudotachylyte from the Homestake shear zone, Sawatch Range, Colorado.

Allen, J.L., and Shaw, C.A., 2011, Seismogenic structure of a crystalline thrust fault: Fabric anisotropy and coeval pseudotachylyte-mylonitic pseudotachylyte in the Grizzly Creek shear zone, Colorado, in, Fagereng, A., Toy, V.G., and Rowland, J., eds., Geology of the Earthquake Source: A Volume in Honour of Rick Sibson: Geological Society, London, Special Publication 359, p.135–151.

Bucher, K., and Frey, M., 1994, Petrogenesis of Metamorphic Rocks: Berlin, Springer-Verlag, p.22

Kirkpatrick, J.D., and Rowe, C.D., 2013, Disappearing ink: How pseudotachylytes are lost from the rock record: Journal of Structural Geology, v.30, p.1-16.

Lee, P.E., Jessup, M.J., Shaw, C.A., Hicks, G.L., and Allen, J.L., 2012, Strain partitioning in the mid-crust of a transpressional shear zone system: Insights from the Homestake and Slide Lake shear zones, central Colorado: Journal of Structural Geology, v. 39, p. 237–252.

Lin, A., 2008, Fossil Earthquakes: The Formation and Preservation of Pseudotachylytes: New York, Springer, p. 23-24.

Maddock, R.H., Grocott, J., and Van Nes, M., 1987, Vesticles, anygdules and similar structures in fault-generated pseudotachylytes: Lithos, v. 20, p. 419-432.

Scholz, C.H., 1990, The Mechanics of Earthquakes and Faulting: Cambridge, Cambridge University Press, p.126, 140-141.

Shaw, C.A., Karlstrom, K.E., Williams, M.L., Jercinovic, M.J., McCoy, A.M., 2001, Electron-microprobe monazite dating of ca. 1.7-1.63 Ga and ca. 1.45-1.38 Ga deformation in the Homestake shear zone, Colorado: origin and early evolution of a persistant intracontinental tectonic zone. Geology 29, p.739-745.

Sibson, R.H., and Toy, V.G., 2006, The Habit of Fault-Generated Pseudotachylyte: Presence vs. Absence of Friction-Melt, in, Earthquakes: Radiated Energy and the Physics of Faulting, Geophysical Monograph Series 170, p. 153-166

Mechanistic study of Toll-Like Receptors during Chlamydia Genital Infection in a Stress Mouse Model

Brandon Kirby

Mentor: Dr. Tesfaye Belay

Bluefield State College

Fall/Spring 2013-14

Abstract

Chlamydia genital infection is the most common sexually transmitted disease (STD) in the United States, with 2.8 million infections occurring annually. If left untreated, complications such as pelvic inflammatory disease (PID) and ectopic pregnancy can arise and lead to infertility. Like most diseases and infections, stress may influence chlamydia genital infection process and the body's defense mechanisms. Toll-like receptors (TLRs) are a family of pattern recognition receptors responsible for the recognition of several pathogen-associated molecular patterns (PAMPs) expressed by the majority of infectious agents. TLR2 and TLR4 have been implicated as receptors mediating cellular activation in response to *Chlamydia trachomatis* however, little is known about the effect of stress and stress hormones on both toll-like receptors. The objective of this study was to examine the gene expression of TLR 2 and TLR 4 in McCoy cells and mice infected with *Chlamydia trachomatis* and subjected to stress protocols. The hypothesis to test was that gene expression profiles of TLR 2 and TLR 4 and the relative magnitude of cytokines are altered by cortisol treatment in *Chlamydia trachomatis* infected McCoy cells and in stressed mice. In a set of experiments, the production of pro-inflammatory cytokines in the genital tracts and spleens of chlamydia-infected stressed or non-stressed mice was examined using RT-PCR and ELISA. PCR data analysis showed increased gene expression of both TLRs infected compared to non-infected cells. Addition of hydrocortisone to McCoy cells infected with *C. trachomatis* resulted in slight increase of mRNA levels of both TLRs. Based on ELISA results, TLR 2, TLR 4 and IL-6 showed higher expression in the stressed compared to non-stressed mice. Based on these results, we can conclude that stress increases the gene expression of key toll-like receptors in mouse genital tract, but the role of both TLRs in cytokine production pathways remains to be explored.

Background and Significance

Genital tract infection caused by *Chlamydia trachomatis* is the most common sexually transmitted disease in the United States with over 2.8 million cases reported annually (Centers for Disease Control and Prevention, 2012). Human ecology and sexual behavior play a dominant role in the spread of bacterial STDs, such as chlamydia (Holmes, 1994). Chlamydia genital infection is found most commonly among 18-24 year olds, with a higher prevalence in low income population. The infection in women (70- 80%) and men (40-50%) is often asymptomatic causing many cases to go unreported and undiagnosed. This could mean that the prevalence of chlamydia is much higher since not all cases are reported. Because of the asymptomatic nature in women, many women will experience irreversible damage to their bodies. Chlamydia can cause permanent scar tissue development in the genital tract and chronic pelvic inflammatory pain if left untreated. These problems can lead to chronic abdominal pain as well as ectopic pregnancy and infertility (Centers for Disease Control and Prevention, 2012).

Chlamydia trachomatis

Chlamydia trachomatis is a gram negative bacterium that is an obligate intracellular organism and has several different serotypes, including D-K that cause urogenital infection and disease. The most common serovars include serovar E and serovar L2, both of which produce different responses in the innate immune system (Dessus-Babus, Darville, Cuozzo, Ferguson, & Wyrick, 2002). *C. trachomatis* infects the epithelial cells of the mucosa lining in the genital tract. These cells are targeted and infected by metabolically inactive elementary bodies that will develop in reticular bodies (Prebeck, et al., 2001). During infection, receptors on the membrane of the infected cells send signals into the nucleus that encode for the production and excretion of molecules that will interact within the immune system to combat the infection.

Infection of *C. trachomatis* can be studied through different cells types, including McCoy cells, and different strains of mice, including BALB/c. McCoy cells are epithelial cells derived from mice that help to simulate the epithelial cells found in the genital tracts.

BALB/c mice are specifically are used and designed to mimic the immune responses found in humans. The infecting dose has been shown to play part in the immune response so the dosage used must be greatly regulated to stimulate the immune response in humans (Maxion, Wei, Chang, & Kelly, 2004).

Toll-like receptors and their functions

Toll-like receptors (TLRs) are classified as *pattern recognition receptors* (PRR) that recognize molecular patterns, referred to as pathogen-associated molecular patterns (PAMPs), located on pathogenic organisms that differ from host molecules and are largely expressed in macrophages and dendritic cells. The molecules recognized by TLRs include lipopolysaccharides, glycoproteins, lipoteichoic acid, etc.

There are thirteen known TLRS present in mammalian cells. Many are located around the membrane of the cell. These receptors are almost all dependent upon the activation of the MyD88 gene. The only TLR independent of this gene is TLR 3. This TLR has been shown to activate separate pathways during up-regulation and is currently being studied in autoimmune diseases (as seen through a summer internship at WVU) (Krasowska-Zoladek, Banaszewska, Kraspulski, & Konat, 2007). TLRs act by sending a signal into the nucleus of the cell through signal transduction. This signal is sent through the activation of many genes, including MyD88 (Pioli, et al., 2004). Once the genes are active, they activate proteins that will regulate several different signaling pathways, including chemokines and cytokines.

TLRs and Chlamydia genital infection: The molecules recognized during infection of *C. trachomatis* are mainly lipopolysaccharides (Erridge, Pridmore, Eley, Stewart, & Poxton, 2004). Dendritic cell functions involving the processing of antigen and presentation to T cells during an infection are largely regulated by TLRs (Kaisho & Akira, 2003). TLR 2 and TLR 4 are responsible for the initial recognition of a chlamydia infection.

TLRs 2 and 4 have been shown to be expressed in the female reproductive tract, the location of a chlamydia infection, during pathogenic challenges (Pioli, et al., 2004). This indicates that these TLRs are largely responsible for the immune response during a chlamydia genital infection. TLR 2 has been shown to play a bigger role in this response compared to TLR 4 during a chlamydia genital infection (Darville, et al., 2003).

Chemokines and Cytokines

Cytokines including chemokines are a type of signaling proteins secreted by cells that can signal for the induction of different responses including inflammation. Different cytokine profiles have been shown to produce different outcomes in chlamydia genital infection (Darville, Andrews Jr, Sikes, Fraley, & Rank, 2001). Chemokines are important mediators in the immune response involving leukocytes (Belay, et al., 2002).

Secretion of these molecules are regulated through a number of cells, including dendritic cells, which are activated by TLRs.

Cytokines Interleukin-6 (IL-6) and Tumor Necrosis Factor-α (TNF-α) have been shown to play direct roles in the immune response of *Chlamydia trachomatis* (Johnson, 2004). IL -6 and TNF-α are co-interacting cytokines with each having an effect on the other. IL- 6 has been identified as a pro-inflammatory cytokine activating inflammation at the site of infection. TNF-α is known to deactivate the effects of IL-6 when in higher amounts than IL-6.

Stress and Infection

Stress has been shown to have a direct effect on the immune system dynamics and its ability to react to pathogenic challenges. Stress has been indicated to suppress the immune system and heighten several infections increasing the associated risks (Khansari & Murgo, 1990). Stress is produced in the body through the release of several hormones, including hydrocortisone or cortisol, from the hypothalamo-pituitary-adrenal-pathway (HPA) and sympathetic nervous system (SNS) (Hawkley & Cacioppo, 2004).

Hydrocortisone suppression has been speculated as having a relationship to the expression of TLRs (Gao, Lin, & Jin, 2009). The effect that stress has on these receptors is unknown. This effect may correlate to the observed differences in chlamydia genital infections since TLRs have a direct role in the immune response of this pathogen.

In order to answer this question, the effect stress and stress hormones must be investigated *in vitro* and *in vivo study* models. A stress mouse model for chlamydia genital infection and immune system analysis has been established in our laboratory and results show that cold-induced stress increases the intensity of chlamydia genital infection associated with immunosuppression in the mouse model. The *in vitro* effect of stress hormone, cortisol on the gene expression of McCoy cells during Chlamydia trachomatis infection was evaluated. Data have shown that addition of cortisol increases the number of detectable inclusions during *C. trachomatis* infection (Bushell & Hobson, 1978). Stress can also be induced in vivo by subjecting mice to a cold water stress protocol. This increases the amounts of stress hormones in the blood of the mice (Jiang & Beller, 1990) (Belay, 2013). The objective of this study was to examine the gene expression of TLR 2 and TLR 4 during Chlamydia infection of McCoy cells treated with hydrocortisone stress hormone and mice subjected to stress protocol. The hypothesis to test was that gene expression profiles of TLR 2 and TLR 4

and the relative magnitude of cytokines and chemokines during *Chlamydia trachomatis* infection of mice are altered by cortisol treatment and cold-stress application.

Materials and Methods

McCoy cell monolayers and growth

McCoy mouse fibroblasts (McCoy cells) were obtained from American Type Culture Collection (ATCC, Manassas, Va). McCoy cell monolayers were grown in 50mL tissue culture flasks containing high glucose Dulbecco's Modified Eagles Medium (DMEM) supplemented with 10% fetal bovine serum, Penicillin-Streptomycin Solution, and Fungizone. Cultures were kept at 37ºC with a 5% CO_2 supply until 80-90% confluent growth for *Chlamydia* isolation

Animals

Six- to seven-week-old female BALB/c mice purchased from Hilltop Lab Animals, Inc.(Scottsdale, PA) were housed in Bluefield State College Basic Science Building room B206 laboratory vivarium. All animal protocols were approved by the Institutional Animal Care and Use Committee of BSC.

Chlamydia trachomatis inoculation to McCoy cells and stress hormone treatment

Monolayers were seeded to 6-well plates and incubated at 37ºC with a 5% CO_2 supply until 95% confluent. Monolayers were infected with 4.2×10^7 IFU/well by centrifuging at 3,000 RPM for one hour then incubating for 2 hours. Supernatant was discarded and replaced with 3 mL complete DMEM containing 100 µg Cortisol (Hydrocortisone; Sigma, St. Louis, MO).

Cold water stress protocol

The cold water stress protocol used was established for inducing physical stress in animals (Jiang & Beller, 1990). Mice were stressed by placing them in a shallow container filled with 4 cm of cold water ($1 \pm 0.5^{O}C$) for 5 minutes each day for 8 days (acute stress). Control mice were not subjected to cold water stress.

Chlamydia trachomatis inoculation protocol to mice

Chlamydia trachomatis mouse pneumonitis agent (MoPn) was obtained from ATCC. *Chlamydia* stock culture contained $1x10^9$ Inclusion Forming Units (IFU)/mL. Seven to ten days prior to infection, mice were injected subcutaneously with 2.5 mg/ mouse in 100 μL of phosphate-buffered saline (PBS) to regulate and sync the mice's menstrual cycles. After the stress induction period, each mouse was infected intravaginally with a working concentration of 10^7 IFU/mL of *C. trachomatis* in 30 μl of PBS while under isoflurane-induced anesthesia.

T cell isolation from spleen cells

The spleens from stressed mice and non-stressed mice were aseptically harvested, placed in a petri dish containing DMEM and held on ice. The weight of each spleen was recorded to determine if production and proliferation of immune cells was affected. The spleens from the stressed mice were pooled and teased to release spleen cells, which contain both B and T cells. T cells were isolated by passing released spleen cells through nylon wool columns (nylon wool loosely packed in a syringe). B cells adhere to the nylon wool, allowing T cells suspended in the media to flow through. The flow- through was collected, centrifuged, and the cell pellet was resuspended in complete DMEM. Cells were counted in a hematocytometer, and the number of cells/mL was determined. T cells were seeded in 96-well tissue culture plates in RPMI media and incubated at 37ºC. Con A was added to the culture to stimulate the production of cytokines and chemokines. Control cells were not exposed to Con A. After 72 hours, the culture supernatant was collected and stored at -20ºC until ELISA assay was performed to test for the presence of cytokines and chemokines in the culture supernatant.

RNA isolation and cDNA synthesis

Total RNA was isolated from McCoy cells using RNeasy Mini Kits from QIAGEN (Valencia, CA). RNA was counted and quality was verified using spectrophotometer. AffinityScript cDNA Synthesis Kits from Agilent Technologies (Santa Clara, CA) were used to synthesize cDNA.

After 48 hours post-infection, euthanasia was carried out by CO_2 inhalation. The genital tracts from stressed or non-stressed mice were harvested and pooled in QIAGEN Allprotect Tissue Reagent to stabilize RNA in the tissue until homogenization. The tissues were disrupted and homogenized in QIAzol Lysis Reagent using a QIAGEN TissueRuptor. Total RNA was extracted from homogenized tissue using a

QIAGEN RNeasy Lipid Tissue Mini Kit following the manufacturer's instructions. RNA quality was verified by gel electrophoresis. cDNA was synthesized using RT^2 First Strand cDNA Synthesis Kit from SABiosciences (Valencia, CA). A small volume of homogenized tissue from stressed and non-stressed mice was saved and stored at -20ºC to be used later.

QRT-PCR analysis of gene expression

The mRNA expression of toll-like receptors and select cytokines from McCoy cell experiment were analyzed using quantitative Reverse Transcriptase Polymerase Chain Reaction (RT-PCR). Primers were purchased from Integrated DNA Technologies, Inc. (Coralville, IA). Brilliant II SYBR Green QPCR Master Mix was used for amplification of cDNA by RT-PCR using a Stratagene Mx3000P PCR system following the manufacturer's protocol.

The mRNA expression of toll-like receptors and proinflammatory cytokines by epithelial cells in the genital tract were analyzed using quantitative Reverse Transcriptase Polymerase Chain Reaction (RT-PCR). DNA amplification by PCR was performed with a Stratagene Mx3000P PCR system using SABiosciences RT^2 Profiler PCR Array: Mouse Inflammatory Cytokines and Receptors following the manufacturer's instructions. The relative levels of mRNA expression were analysed by comparison of the threshold cycle during which fluorescence was detected. Fold change and fold up- or down- regulation of the mRNA expression of cytokines, chemokines and chemokine receptors was calculated to determine if there were significant differences in the expression of these molecules and to determine statistical significance of the data.

Gel image analysis

Amplified DNA in PCR products was electrophoresed in a 2% gel. Relative amounts of product for selected cytokines, chemokines, and chemokine receptors were examined using gel image analysis. The intensities of the bands produced in the gel were compared. In general, the higher the intensity of the band, the higher the concentration of the target molecule is in the sample.

Enzyme Linked Immunosorbent Assay

The levels of Interleukin-6 and Tumor Necrosis Factor- α present in genital tract and spleen homogenates were quantified by ELISA using kits from Invitrogen (Grand Island, NY). Levels of cytokines were measured using an ELISA plate reader>

Results

The gene expression profiles of TLRs 2 and 4 in McCoy cells inoculated with *Chlamydia trachomatis* were compared with non-infected cells (Figures 1a and 1b). Cortisol was also added into both groups to compare and determine the effect of stress hormones. In cells that were infected, TLRs 2 and 4 both showed up-regulation. In cells that were infected with cortisol in the media, TLRs 2 and 4 showed further up-regulation compared to just the infected model. This provided a basis that stress hormones further up-regulate TLRs and may over-activate different signaling pathways to produce various immune responses. This data offered sufficient evidence to move onto in vivo studies.

The gene expression profiles of TLRs 2 and 4 in the genital tracts of mice that were infected with chlamydia and stressed for 21-24 days using a cold water stress protocol were compared with non-stressed mice using RT-PCR (Figures 2a and 2b). In mice that were stressed, there was an up-regulation of both TLRs 2 and 4 compared to the non-stressed. The TLR 2 mRNA in the stressed mice was up-regulated about six-to-seven thermal cycles ahead of the non-stressed TLR 2 mRNA. The TLR 4 mRNA of the stressed mice was also up-regulated about six-to-seven thermal cycles ahead of the TLR 4 mRNA in the non-stressed mice. These results followed suit with the data delivered through RT-PCR and gel electrophoresis in the McCoy cell models and gave sufficient evidence to study the effector mechanisms, such as cytokines, produced through the activation of the TLR pathways.

The gene expression profiles of cytokines IL-6 and TNF-α were compared using RT- PCR from the same mice used to study the gene expression profiles of TLRs 2 and 4 (Figures 3a and 3b). There was up-regulation of the pro-inflammatory cytokine IL-6 mRNA about five-to-six cycles ahead of the non-stressed model. The anti-inflammatory cytokine TNF-α mRNA was down-regulated in the stressed model with the non-stressed TNF-α mRNA expressing about ten+ cycles ahead. This data provided interest to study the production levels of the cytokines.

The production of cytokines in the genital tract was studied using ELISA in the stressed and non-stressed infected mouse models (Figure 4). The anti-inflammatory cytokine TNF-α was in higher concentration in the non-stressed model, whereas the pro- inflammatory cytokine IL-6 was in a much higher concentration in the stressed model. This result followed the RT-PCR profiles of the cytokines and gave evidence of increased inflammation in the stressed model.

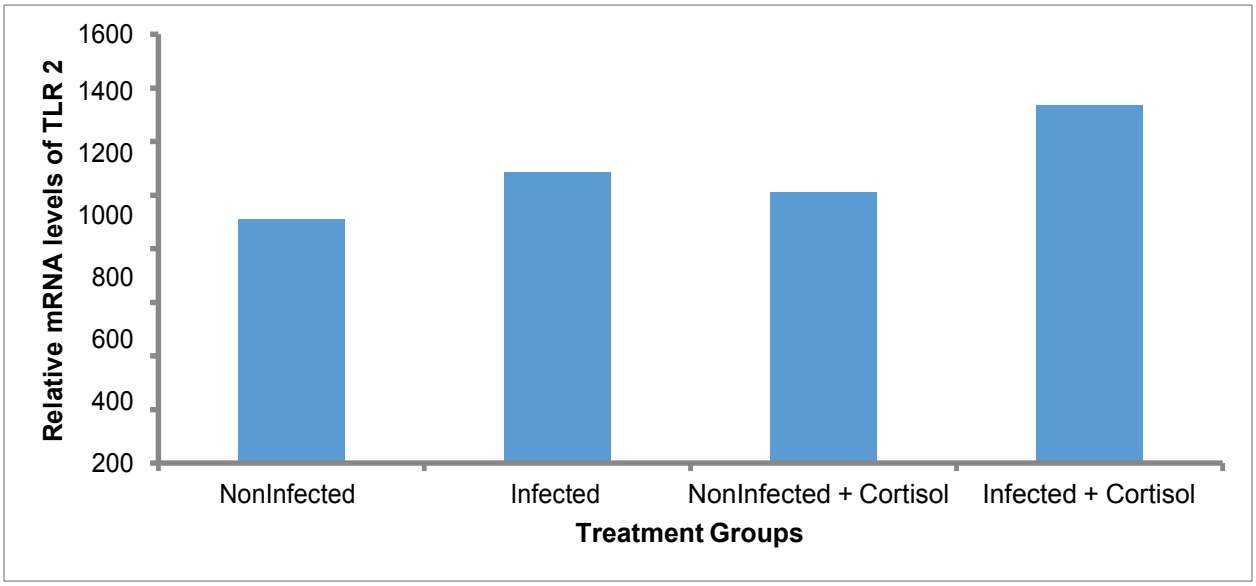

Figure 1a: Effects of cortisol on the gene expression of TLR 2 in McCoy cells infected with *Chlamydia trachomatis.* Data collected using spectrophotometry of gel electrophoresed RT-PCR product.

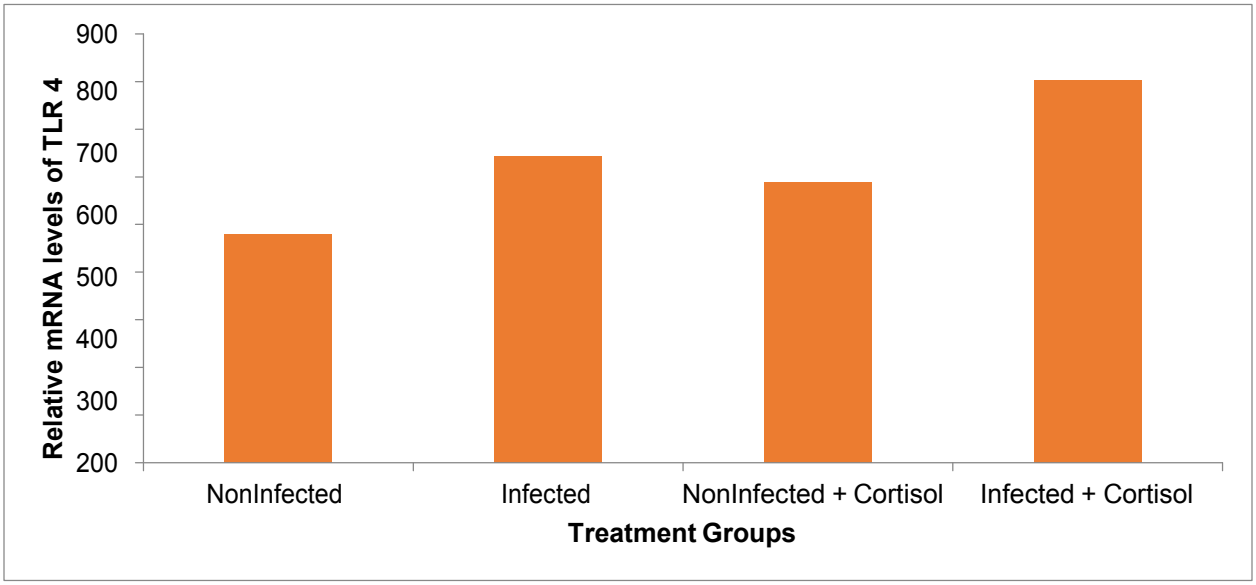

Figure 1b: Effects of cortisol on the gene expression of TLR 4 in McCoy cells infected with *Chlamydia trachomatis*. Data collected using spectrophotometry of gel electrophoresed RT-PCR product.

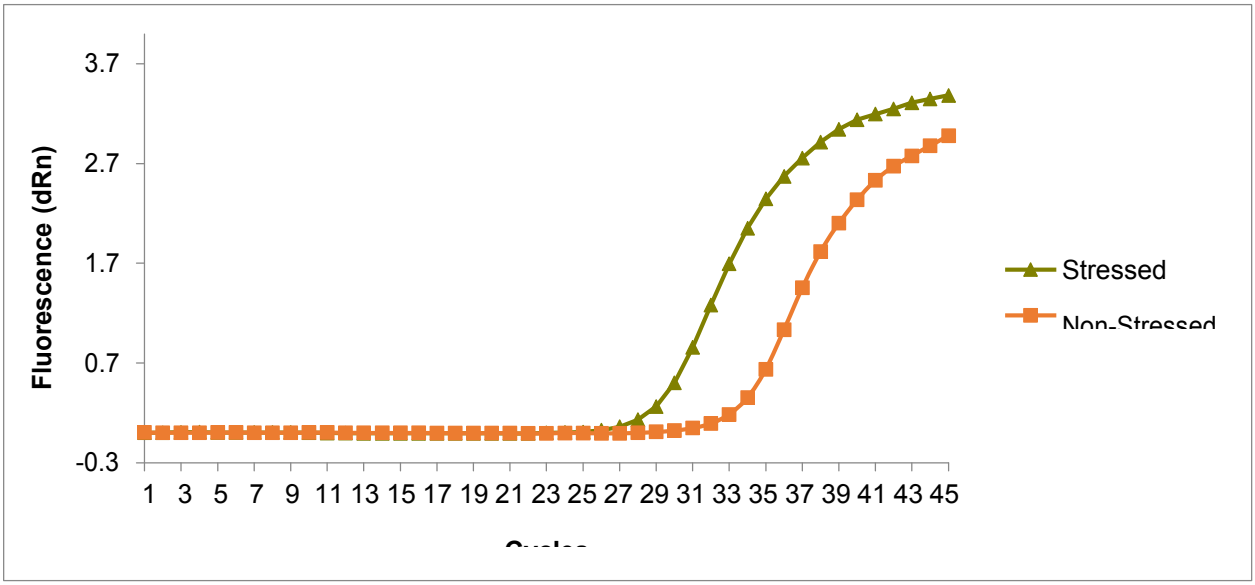

Figure 2a: Gene expression profiles of TLR 2 in the stressed infected and non-stressed infected mice. Data collected using real time RT-PCR..

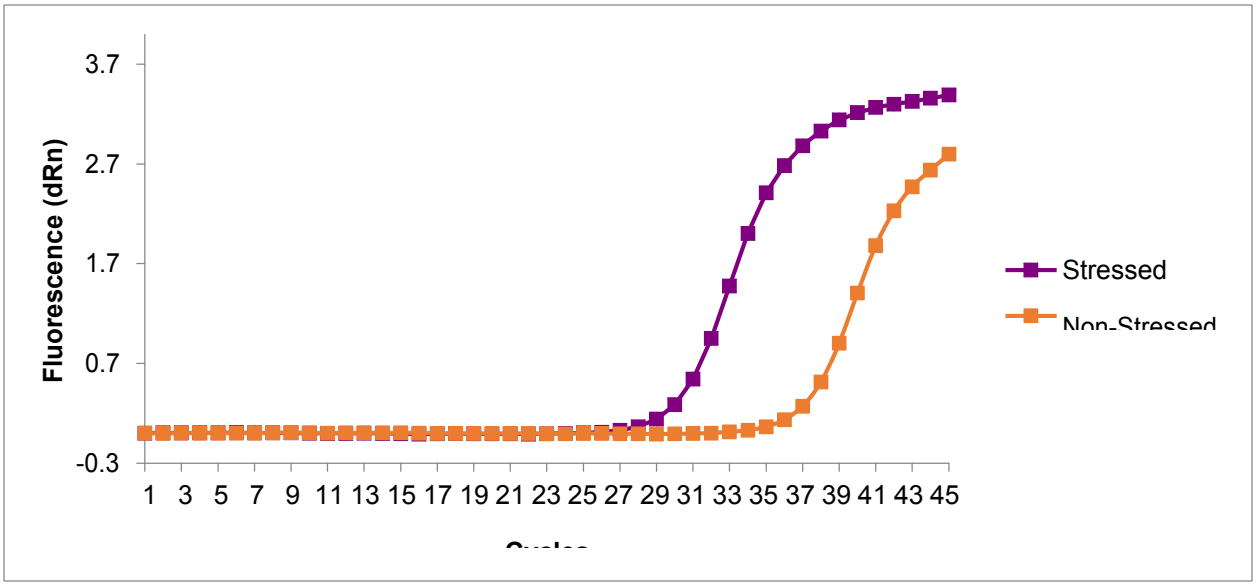

Figure 2b: Gene expression profiles of TLR 4 in the stressed infected and non-stressed infected mice. Data collected using real time RT-PCR.

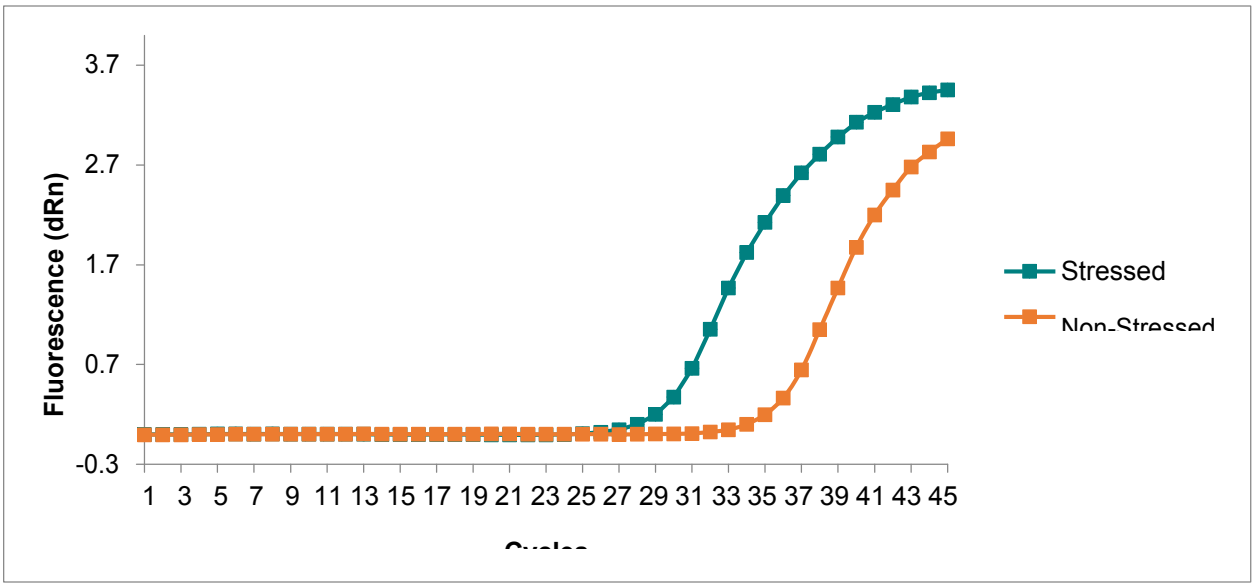

Figure 3a: Gene expression profiles of IL-6 in the stressed infected and non-stressed infected mice. Data collected using real time RT-PCR.

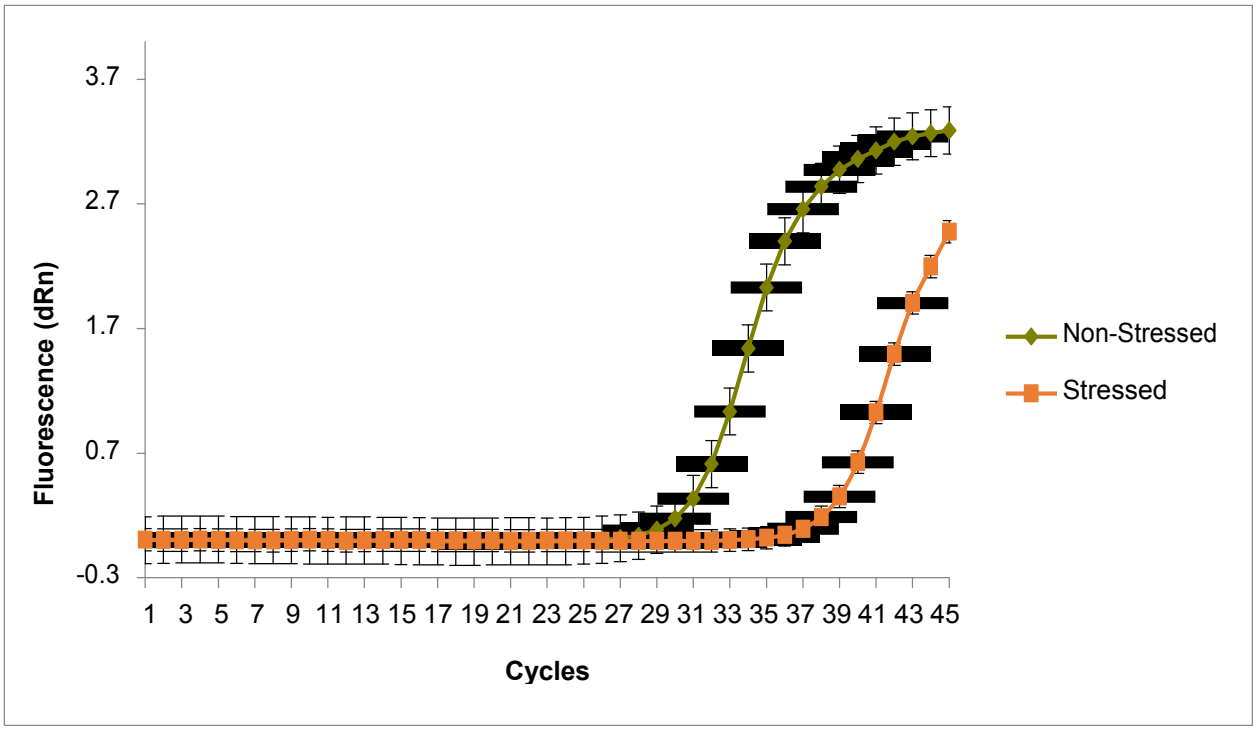

Figure 3b: Gene expression profiles of TNF-α in the stressed infected and non-stressed infected mice. Data collected using real time RT-PCR.

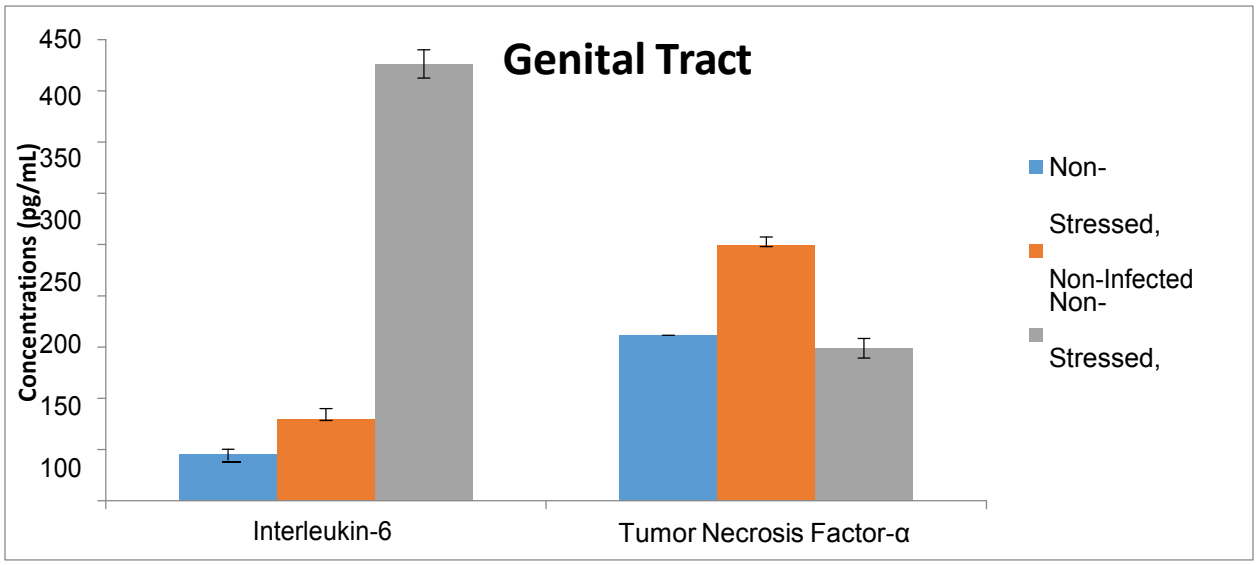

Figure 4: Production levels of cytokines in the genital tracts of non-stressed/non-infected, non- stressed/infected, and stress/infected mice. Data collected using ELISA plate and plate reader.

Conclusion

Stress plays and major role in almost any infection. Stress has been shown in this study to increase and alter the expression of TLRs 2 and 4 during a Chlamydia genital infection, which lead to the overproduction of inflammatory cytokines in the genital tract. The presence of these inflammatory cytokines suggests that a stressed infection would be more severe with an increasing amount of inflammation. The pathways activated through TLRs that are responsible for various immune responses are expected to be over-activated. This could lead to increased and more severe immune responses and could explain many chronic diseases associated with *Chlamydia trachomatis* such as pelvic inflammatory disease and chronic inflammation. The pathways of TLRs to the cytokines remains to be explored to determine the exact correspondence of TLRs and the cytokines studied. Future studies will be focused around transcription factors such as NF-κB and specific genes located in the TLR pathways including MyD88.

Acknowledgements

This study was supported by the McNair Program at Concord University, the WV-INBRE grant, and Bluefield State College. Special thanks to Dr. Tesfaye Belay at BSC and the McNair staff at CU.

References

Belay, T., Eko, F. O., Ananaba, G. A., Bowers, S., Moore, T., Lyn, D., & Igietseme, J. U. (2002). Chemokine and Chemokine Receptor Dynamics during Genital Chlamydia Infection. *Infection and Immunity*.

Bushell, A. C., & Hobson, D. (1978). Effect of Cortisol on the Growth of *Chlamydia trachomatis* in McCoy Cells. *Infection and Immunity*, 946-953.
Centers for Disease Control and Prevention. (2012, November 29). *Chlamydia - CDC Fact Sheet*. Retrieved from CDC: http://www.cdc.gov/std/chlamydia/STDFact-chlamydia- detailed.htm

Darville, T., Andrews Jr, C. W., Sikes, J. D., Fraley, P. L., & Rank, R. G. (2001). Early Local Cytokine Profiles in Strains of Mice with Different Outcomes from Chalmydial Genital Tract Infection. *Infection and Immunity*, 3556-3561.

Darville, T., O'Neill, J. M., Andrews Jr, C. W., Nagarajan, U. M., Stahl, L., & Ojcius, D. M. (2003). Toll-Like Receptor-2, but Not Toll-Like Receptor-4, Is Essential for Development of Oviduct Pathology in Chlamydial Genital Tract Infection. *The Journal of Immunology*, 6188-6197.

Dessus-Babus, S., Darville, T. L., Cuozzo, F. P., Ferguson, K., & Wyrick, P. B. (2002). Differences in Innant Immune Responses (In Vitro) to HeLa Cells Infected with Nondisseminating Serovar E and Disseminating Serovar L2 of *Chlamydia trachomatis*. *Infection and Immunity*, 3234-3248.

Erridge, C., Pridmore, A., Eley, A., Stewart, J., & Poxton, I. R. (2004). Lipopolysaccharides of *Bacteroides fragilis*, *Chlamydia trachomatis*, and *Pseudomonas aeruginosa* signal via Toll-like receptor 2. *Journal of Medical Microbioloy*, 735-740.

Gao, T., Lin, Z., & Jin, X. (2009). Hydrocortisone Suppression of the Expression of VEGF May Relate to Toll-Like Receptor (TLR) 2 and 4. *Current Eye Research*, 777-784.

Gervassi, A., Alderson, M. R., Suchland, R., Maisonneuve, J. F., Grabstein, K. H., & Probst, P. (2004). Differential Regulation of Inflammtory Cytokine Secretion by Human Dendritic Cells upon *Chlamydia trachomatis* Infection. *Infection and Immunity*, 7231-7239.

Hawkley, L. C., & Cacioppo, J. T. (2004). Stress and the aging immune system. *Brain, Behavior, and Immunity*, 114-119.

Holmes, K. K. (1994). Human ecology and behavior and sexually transmitted bacterial infections. *Proceedings of the National Academy of Sciences*, 2448-2455.

Jiang, C. G., & Beller, D. I. (1990). Immunosupression in mice induced by cold water stress. *Brain, Behavior, and Immunity*, 278-279.

Johnson, R. M. (2004). Murine Oviduct Epithelial Cell Cytokine Responses to *Chlamydia muridarum* Infection Include Interluekin-12-p70 Secretion. *Infection and Immunity*, 3951- 3960.

Kaisho, T., & Akira, S. (2003). Regulation of Dendritic Cell Function Through Toll-like Receptors. *Current Molecular Medicine*, 373-385.

Khansari, D. N., & Murgo, A. J. (1990). Effects of stress on the immune system. *Immunology Today*, 170-175.

Krasowska-Zoladek, A., Banaszewska, M., Kraspulski, M., & Konat, G. (2007). Kinetics of inflammatory response of astrocytes induced by TLR 3 and TLR 4 ligation. *Journal of Neuroscience Research*, 205-212.

Maxion, H. K., Wei, L., Chang, M.-H., & Kelly, K. A. (2004). The Infecting Dose of *Chlamydia muridarum* Modulates the Innate Immune Response and Ascending Infection. *Infection and Immunity*, 6330-6340.

Pioli, P. A., Amiel, E., Schaefer, T. M., Connolly, J. E., Wira, C. R., & Guyre, P. M. (2004). Differential Expression of Toll-Like Receptors 2 and 4 in Tissues of the Human Female Reproductive Tract. *Infection and Immunity*, 5799-5806.

Prebeck, S. K., Durr, S., de Costa, C., Donath, B., Brand, K., Redecke, V., . . . Miethke, T. (2001). Predominant Role of Toll-Like Receptor 2 Versus 4 in *Chlamydia pneumonia*- Induced Activation of Dendritic Cells. *The Journal of Immunology*, 3316-3323.

Sexual Orientation Discrimination in the Hiring Process: A Study on Stereotypes

Laken C. McKenzie

Concord University

Sexual Orientation Discrimination in the Hiring Process: A Study on Stereotypes

Discrimination by employers during the hiring process and to employees in the workplace is not a new phenomenon. Women and African Americans share problems such as lower salaries and fewer offers of leadership positions, and they often experience a more difficult time even getting hired for a job (McConahay, 1983) (Cortina & Holland, 2013). One of the more well-known studies involving discrimination among African American men showed that while white men with a criminal record received fewer callbacks than white men without records, even those white men with criminal records still received more callbacks than African American men without records (Pager 2003). With all the recent attention given to marriage equality for gays, lesbians, and transsexuals other plights of the LGBT community are often overlooked. One such disadvantage is discrimination in both the hiring process and in the workplace for gays, lesbians, and transsexuals.

Homosexuality was considered a mental disease by the American Psychiatric Association until 1973, and thus, few studies have been conducted to try and find patterns of discrimination against the LGBT community. Adam (1981) was one of the first studies to use correspondence testing regarding discrimination against LGBT in the workplace. Correspondence testing is when applications which are mostly identical except for the studied variable are sent to different openings. When one applicant is chosen repeatedly over the one with the variable it is attributed to discrimination. Although he received fewer callbacks for his homosexual applicants thus supporting his hypothesis, his study was small. Hebl et. al (2002) conducted an in-person audit study with 84 employees in a mall setting. Studies using in-person audit methodology are more generalizable and provide more evidence to discrimination in the workplace than other studies. Hebl et al's (2002) study also found evidence to support discrimination, yet it also had a

relatively small sample size.

As with any study, operational definitions of terms is one of the biggest concerns and when studying discrimination against a discreditable trait it is important to understand how the person obtains the deviant title of homosexual, bisexual, or transgendered. Goffman (1963) distinguished two types of stigma: discreditable and discredited. He stated that discredited traits are traits that are often physical in nature, such as a deformity, race, or handicaps, which are easily identified by others. Discreditable traits, however, are traits that are more invisible to the public, such as religion, criminal history, or homosexuality. In the current study, I will focus on discrimination against lesbians in a hiring situation. To attach the label of homosexual through social stigma, one applicant will be a member of their University's LGBT organization. Tilcsik (2011) describes stereotypes as shared sets of explicit or implicit traits of a social, ethnic, or other group as seen by society. Thus there must be a distinction among four types of women through stereotypes. Weichselbaumer (2001) classified women as straight feminine, straight masculine, lesbian feminine, or femme, and lesbian masculine, or butch. In her study Weichselbaumer created the homosexual label through manipulation of clothes, hairstyle, and atmosphere of a picture that was sent with the job applications. An example would be a woman dressed in a suit with a short, business haircut versus a woman in an evening dress with long hair in a work bun. Since this study took place in Australia where a picture must be included with each application, it was not unusual. Weichselbaumer found that there was discrimination against any masculine women and feminine women with a homosexual label (Weichselbaumer 2001).

Drydakis (2009) found another way to indicate sexual orientation without using visual stereotypes. On the resumes, Drydakis mentioned the applicant was "active in the Athenian Homosexual Community" and the results showed only 14% of the homosexual applicants were

called back while 40% of the control group was called back. In 2011, Drydakis conducted another study regarding discrimination against lesbians. In the study, two women were sent out with equal human capital resumes and one with a homosexual indicator. The results showed a correlation between sexual orientation and discrimination. Drydakis attributes these findings in part to the sexual stigma, or society's shared disregard for any behavior, identity, relationship, or community that is not heterosexual, found in Greece (Drydakis 2011).

This study relies on a pseudo hiring situation where the participant is given two applications and then asked which one they would hire and why they would hire that applicant. The participant will be placed in either Group Control or Group Experimental without their knowledge. Group Experimental will receive one application with the homosexual indicator. Membership in the local LGBT organization will be the homosexual indicator for Group Experimental. The hypothesis of this study is that more participants will chose the heterosexual applicant over the homosexual applicant in Group Experiment, and that the participants will choose the two heterosexual applicants in Group Control relatively equally.

Method

Participants

There were 100 participants in the study. They were all college students from intro level courses between the ages of 17 and 48 with 42% females, 55% males, and 3% other. The majority of the participants were white, 74%, heterosexual, 97%, and between the ages of 18-21, 91%. Every participant was given the option to participate with no effect on their grade and they were all informed of confidentiality and the right to participation.

Materials

The study was conducted using a pencil and paper survey attached to two applications. The survey contained questions about demographic background such as age, sex, race, sexual orientation, and year in college. The final part of the survey contained questions concerning the applications. The participants were asked which applicant they would hire, which applicant had better credentials, and they had the opportunity to answer an open question which asked for the reasons of their choices. There were three different applications. Group Control was given Application One with no homosexual marker, while Group Experimental was given Application One with a homosexual indicator in the form of a leadership position in the University's LGBT club. Both groups were given the same Application Two. Both applications contained pseudo background information, education, certifications, work experience, and professional organizations. The two applications were also formatted to contain equal human capitol without containing identical information. The study was approved by the University Human Subject Review Board prior to conduction the research.

Procedure

The surveys were stapled to a set with two heterosexual applications or to a set with one heterosexual application and one application with the homosexual indicator. Then the surveys were passed out in an alternating pattern to evenly distribute the groups. The participants were instructed to read the two applications then answer all the questions on the survey and the participants were informed of their rights to confidentiality and their right to participate. After completion, the surveys were collected by the researcher.

Results

The data was analyzed using a chi-square test and showed no statistically significant relationship between Group Control and Group Experimental, phi=.077 and p<.445. Group Control chose Application One 42.30% and Application Two 57.70%. Group Experimental chose Application One 34.80% and Application Two 65.20%.

Discussion

Although the results were not statistically significant, the patterns observed does support the hypothesis. Participants in Group Experimental were more likely to choose the heterosexual individual, 65.20%, than the homosexual individual, 34.80%, and participants in Group Control choose both individuals relatively equally, 42.30% and 57.70%. If more participants were involved, or if the study took place in more diverse environments, the pattern of results may become statistically significant. The data may also change depending on the cultural background of the area where the data is collected. Some states and countries are more progressive in equal rights for minorities of all types, while other states and countries still place a social stigma on those individuals in the workplace.

Studies, such as the one conducted, are important for social scientists who research gender issues and disruptions in society due to sexual orientation discrimination. Studies in a real world setting can be used to illuminate the discrimination faced by members of the LGBT community all over the world. Perhaps with more research being conducted, equality in all forms, not just marriage, can be achieved by minorities that include members of the LGBT and by women and racial minorities. Only through understanding the reality of the difficulties these groups go through will anything change for the better.

References

Adam, Barry D. (1981). Stigma and employability: discrimination by sex and sexual orientation in the Ontario legal profession. *Canadian Review of Sociology and Anthropology, 18 (2),* 216 – 221.

Cortina, L. Holland, K. (2013). When sexism and feminism collide: The sexual harassment of feminist working women. *Psychology of Women Quarterly. 37,* 129-208.

Drydakis, N. (2009). Sexual orientation discrimination in the labour market. *Labour Economics, 16,* 364-372.

Drydakis, N. (2011). Women's sexual orientation and labor market outcomes in Greece. *Feminist Economics, 17,* 89-117.

Goffman, E. (1963). *Stigma*. S.l.

Hebl, Michelle R., Jessica Bigazzi Foster, Laura M. Mannix, and John Dovidio. (2002). Formal and interpersonal discrimination: a field study of bias toward homosexual applicants. *Personality and Social Psychology Bulletin, 28,* 815–25.

McConahay, J. (1983). Modern racism and modern discrimination: The effects of race, racial attitudes, and context on simulated hiring decisions. Duke University.

Pager, D. (2003). The mark of a criminal record. *American Journal of Sociology, 108,* 937-975.

Tilcsik, A. (2011). Pride and prejudice: employment discrimination against openly gay men in the United States. *American Journal of Sociology, 117 (2),* 586-626.

Weichselbaumer, D. (2001). Sexual orientation discrimination in hiring. Johannes Kepler University of Linz.

Malaria Infection Simulation Model

Musa Nyassi

Mentor: Adem Ozyavas

Abstract

This project uses computer models and NetLogo, an agent-based modeling and simulation toolbox, to study the spread of Malaria in a population and the effect of different human intervention strategies. Simulation and Visualization on how Malaria spreads in a population not only shows how people get infected by mosquitoes carrying Malaria causing plasmodium parasites and eventually getting sick, it can also be a meaningful tool in disease prevention. One can isolate a variable which contributes to perpetuation of the disease and analyze if the disease spread can be circumscribed or stopped. In this project we studied the effect of various intervention strategies: the use of mosquito nets, cleanliness of the environment, the use of insecticides; other variables were also incorporated into the model: the seasons (rainy or dry seasons) and immunity.

Introduction

This project refines a previously started computer model, which simulates the spread of Malaria in a population. It uses NetLogo, an agent-based modeling and simulation toolbox, to study the spread of Malaria in a population and the effect of different human intervention strategies.

Simulation and Visualization on how Malaria spreads in a population not only shows how people get infected by mosquitoes carrying Malaria parasites and eventually getting sick, it can also be a meaningful tool in disease prevention.

The project is more of an endeavor to capture a biological process and simply present or illustrate it using a computer model, drawing from programming methodologies and adhering to software development practices.

Simulating Malaria Infection

Malaria is still a major health problem in many parts of the world, especially in Sub-Saharan Africa. It kills many people every year around the world. For me, Malaria strikes very close to home, as I have on numerous occasions fallen victim to its rancor. According to the World Health Organization, in 2010 alone, there were about 216 million cases of malaria and an estimated 655,000 deaths. Majority of these deaths occur among children living in Africa where a child dies every minute from malaria (WHO). It is caused by Plasmodium parasites, which are spread to people through the bites of infected Anopheles mosquitoes, called "malaria vectors", which bite mainly between dusk and dawn. The mosquito, thus remains pivotal in the spread of Malaria, it is the link between humans and the malaria causing plasmodium parasite.

The model therefore aims to simulate the spread of Malaria in a human population; taking into account the various variables which perpetuate and hinder the spread of the disease with a view to understand how these variables influence the disease's perpetuation and/or prevention.

A model simulation thus greatly helps users gain a better understanding of the disease's epidemiology and to make plans for the corresponding prevention. One can isolate a variable which contributes to perpetuation of the disease and analyze if the disease spread can be circumscribed or stopped. The project studies the effect of three intervention strategies: mosquito nets, a clean environment and the use of insecticides already. Additional strategies and variables will be included in the model to give it a more realistic representation of the spread of infection. These include differentiating the environment into two distinct seasons; rainy and dry season, as malaria prevalence fluctuates between these seasons. Immunity will be included so as represent that portion of the population that has developed immunity. Lastly put in a mechanism to keep track of the duration of infectiousness, to help determine how long someone has been sick, and hopefully chart a course of action based off on that.

Analyzing a real world problem and building a computer program to help study and gain a better understanding of a problem will surely will engage the skills and knowledge I gained over the course of my computer science studies at Bluefield State College.
Below is the project time line:

MALARIA INFECTION SIMULATION MODEL	
Period	Milestone Deliverables
06/15/13 – 07/15/13	- Finish project proposal; detailing project nature, plan and direction
07/04/13 – 09/18/13	- Identify more variables that perpetuate infection - Identify intervention strategies - Complete information gathering, articles and papers on Malaria
10/18/13 – 10/04/13	- Finish pseudo code for NetLogo
10/04/13 – 10/18/13	- Finish writing program/procedures for simulation
10/18/13 – 11/01/13	- Test programs; simulate and record results - Debugging & Troubleshooting
11/01/13 – 11/15/13	- More trouble shooting and debugging
11/15/13 –11/29/13	- Finish final report - Consult with mentor
11/29/13 – 12/06/13	- Finish research paper - PowerPoint Presentation

Literature Review

The Malaria model runs on NetLogo, a programmable modeling environment for simulating natural and social phenomena. It has been in continuous development ever since at the Center for Connected Learning and Computer-Based Modeling. NetLogo is touted to be particularly well suited for modeling complex systems developing over time. Modelers can give instructions to hundreds or thousands of 'agents' all operating independently. This makes it possible to explore the connection between the micro-level behavior of individuals and the macro-level patterns that emerge from their interaction. [Wilensky]. NetLogo comes with many models to simulate various phenomena, ranging from Biology to Social Science giving one a head start as to how to apply or extend some of the already existing models or come up with new models. Among these default models; three are of interest to the Malaria model; which generally simulate the spread of diseases between agents and within populations with different variables which profoundly affect the spread of such diseases: a virus model, a disease-solo model and an HIV- Aids model.

The Virus model simulates people moving randomly about the world in one of three states: healthy but susceptible to infection (green), sick and infectious (red), and healthy and immune (gray). People may die of infection or old age. Sick people may infect healthy people when they come in contact, healthy people may reproduce.

In the Disease solo model simulation, one agent in the population is a person controlled by the user; the others are "androids" controlled by the computer. A user controls when infection starts or ends, whether sick agents should chase healthy agents or healthy agents should run from the sick agents.

The HIV AIDS model simulates the spread of the human immunodeficiency virus (HIV), via sexual transmission, through a small isolated human population. It therefore illustrates the effects of certain sexual practices across a population.

The Malaria model on the NetLogo platform therefore simulates what happens when the various variables which affect the spread of Malaria in the population are tweaked around, in a host, agent and environment triad. It does draw many basic procedures from the above models with further additions of its own.

Among its variables is the use of mosquito nets, a clean environment, and access to health facilities or medication. The WHO report stipulates that, “vector control is the main way to reduce malaria transmission at the community level. It is the only intervention that can reduce malaria transmission from very high levels to close to zero.” The two most effective methods of mosquito control are the use of Insecticide-treated mosquito nets (ITNs) and Indoor spraying with residual insecticides. The model will however put more emphasis on the use of mosquito nets, a clean environment, insecticide usage, time of the year (whether dry or rainy season) and their effects on the spread of the disease.

Methodology

Since NetLogo is an agent-based modeling platform: comprising of turtles, patches, links, and the observer. Turtles move around in the space. The space is two dimensional and is divided up into a grid of patches. Each patch is a square piece of "ground" over which turtles can move. Links are connections between turtles. The observer doesn't occupy a position within the space; it can be imagined as looking out over the world of turtles and patches.

All the players involved in the Malaria infection-prevention cycle i.e. persons, mosquitoes and clinics were created out of “turtles”; we created different “breeds” of the turtle agent to represent each one of them. Thus we had persons, mosquitoes and clinics breed.

A person exists in four states: healthy – either never infected or infected but recovered; immune – never get infected; sick – infected with the plasmodium parasites; dead – died because of the disease.

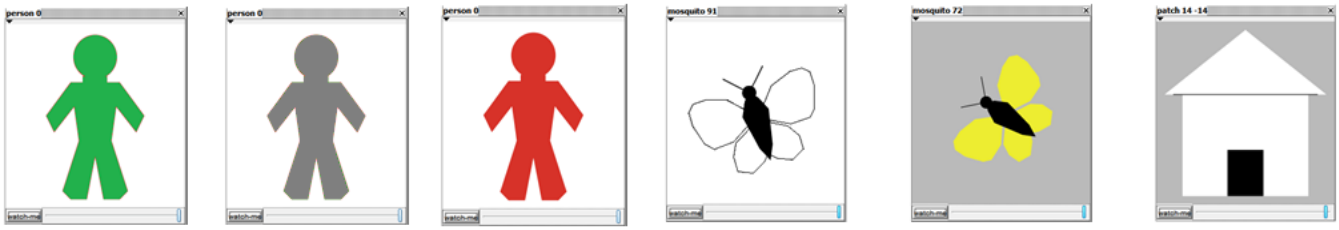

Figure 1 Breeds of turtles in the population

A mosquito exists in three states: infective – carrying the parasite; non-infective – not carrying the parasite and therefore not infectious; dead – lifespan. The infective mosquitoes may cause persons to become sick whenever they come in contact with them. A non-infective mosquito may also become infective when it bites a sick person.

Initially five Clinics were positioned in the four corners of the environment and at the, but with further development, one can now assign a reasonable number of clinics, this can be adjusted according to reflect the number of clinics or health facilities

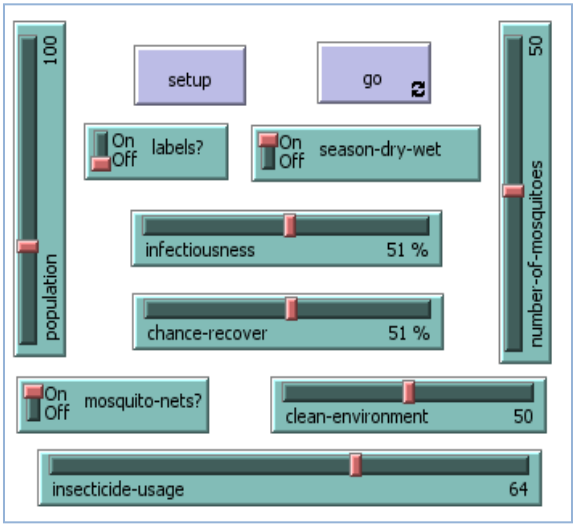

Figure 2 User interface (variables)

accessible to a population during a simulation, it should be noted that the ratio of clinics to people differs from place to place. So the ability to vary this was deemed to be very important.

While some parameters were hardcoded (set to default values) in the program, many were left to the user's discretion. The interface was setup to present to the user those variables which can be initialized or modified before every run. These were the initial number of people in the population, the initial number of mosquitoes, the infectiousness of the disease (the higher the number the greater the chance of infection), chance of recovery after being infected (the higher the number, the greater the chance of getting well after visiting a clinic), a switch to indicate whether mosquito nets are being used in the population or not; two sliders for clean-environment and insecticide usage to set the level of cleanliness and insecticide usage in the population respectively. When these variables are set; successful runs can be initiated and readings are recorded accordingly.

Simulation

Our approach in the design of the model lies in a closed knit population where people and mosquitoes can move around randomly in 2D. In real life, people don't just wander around randomly without a purpose; they frequent certain locations than others. Places of work, school, business, recreation, entertainment, etc are mostly frequented. Neither do mosquitoes fly around randomly. Therefore, it is still a mathematical model which ignores certain aspects of disease spread; mathematical models are by nature a simplification of the problem. It is thus important to bear in mind the underlying assumptions.

A person has two parameters, a *sick?* Boolean variable and *sick-days* count variable, the former indicates the state of the person; whether he is sick or not while the former keeps count of the number of days a person has been sick. Whenever the number of sick days goes above a threshold without seeking medical attention or going to one of the five clinics, the person eventually succumbs to the disease.

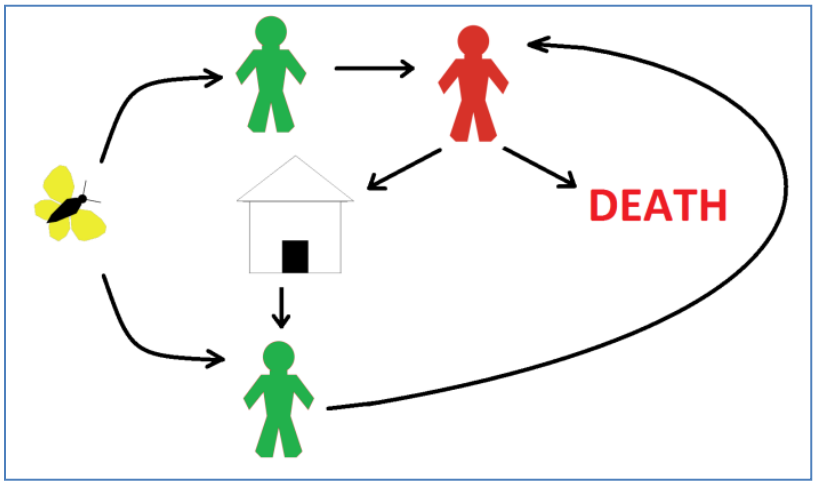

Figure 3 Infection-cycle of a person

Mosquitoes also have two parameters, an *infected?* Boolean variable which determines whether a mosquito is infective or not and a life variable which holds the amount of life a mosquito possesses. At initialization and subsequently at birth mosquitoes are given a *life* count, when they fly around and bite persons their life counts goes up (reflecting feeding and growth) and when it reaches a certain threshold they may reproduce.

On the other hand, when mosquitoes move about without biting or feeding on people their life counts dip, eventually reaching a life count of zero results to death. Thus their survival depends on biting people. The probability for

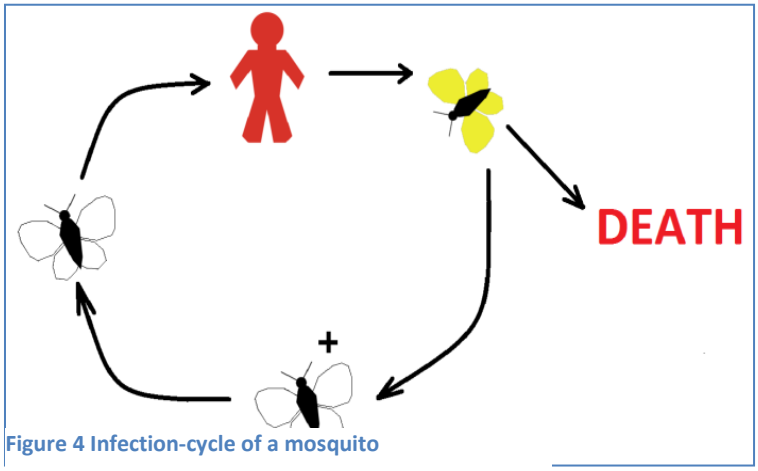

Figure 4 Infection-cycle of a mosquito

the infective mosquitoes to bite and cause sickness is tied to the use of mosquito nets while their probability for reproducing new offspring is tied to the use of insecticide in the population.

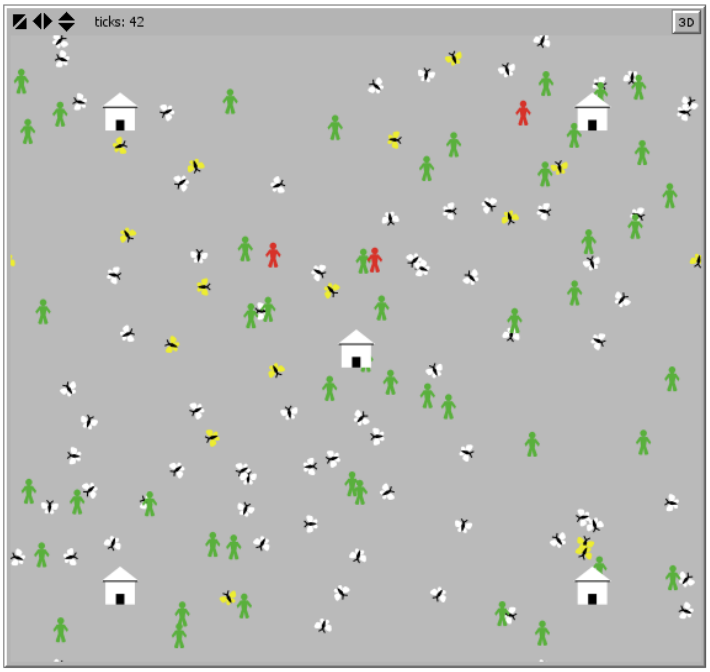

Figure 5 A simulation in progress, population screenshot

In a typical run or scenario initiated after the parameters (Fig. 2) are adjusted for the stochastic simulation. Healthy people move around, get infected, recover (the probability to recover depends on getting to a clinic as early as possible and also on the chance-recover parameter) or they die after contracting the disease for a certain number of days. At the same time mosquitoes also fly around, bite, carry the plasmodium parasite, bite and feed off them, reproduce or if they are not able to bite or feed, they starve and die.

In the procedures or code behind, every person is assigned a number of variables (containers that hold values); these variables hold different values for each person at every point in time during the simulation. The *sick?* Boolean variable determines whether or not a person is sick; the *immune?* Boolean variable determines whether a person is immune or not; while the *sick-days* integer variable keeps track of the number of days a person, once infected has been carrying the disease. Each person agent also calls on several procedures, the *move-persons* procedure is a function that determines how a person moves; there is also the *get-sick*, *move-to-treatment*, *get-treatment and* death-persons.

Mosquitoes too are assigned several variables and call on mosquito specific procedures or functions. Each mosquito has a *life* integer variable, which keeps track of how long it has been in the environment, they all call on *move-mosquitoes*, *mosquito-bite*, *get-infected*, *death-mosquitoes* and *reproduce-mosquitoes* procedures. Certain actions trigger some of the procedures though, for example a mosquito calls the mosquito-bite procedure when it comes in contact with a person.

Clinics basically have a single variable: *give-treatment*, to treat persons with Malaria. There are other procedures which initialize what a person should look like, i.e. assigning different images, colors and sizes to the different breeds (persons, mosquitoes and clinics), these initial values also set various environment parameters, size and dimension (2D or 3D) and also set the initial number of infected persons and mosquitoes.

Results

Figure 5 shows a screenshot of the simulation. People and mosquitoes continuously move about and carry on things they do after every “tick”, in many NetLogo models, time passes in discrete steps, called "ticks".

At 400 ticks (about 13.3 months; ticks/30, 1 tick = 1 day); we did 100 runs, half of them with the most conducive environment present for the disease to spread and the other half with unfavorable conditions for the disease to spread. It was observed that over time and on average more people remained healthy and fewer people got infected when mosquito nets were used, in a clean environment and more insecticide usage than when these variables were set to mimic unfavorable conditions.

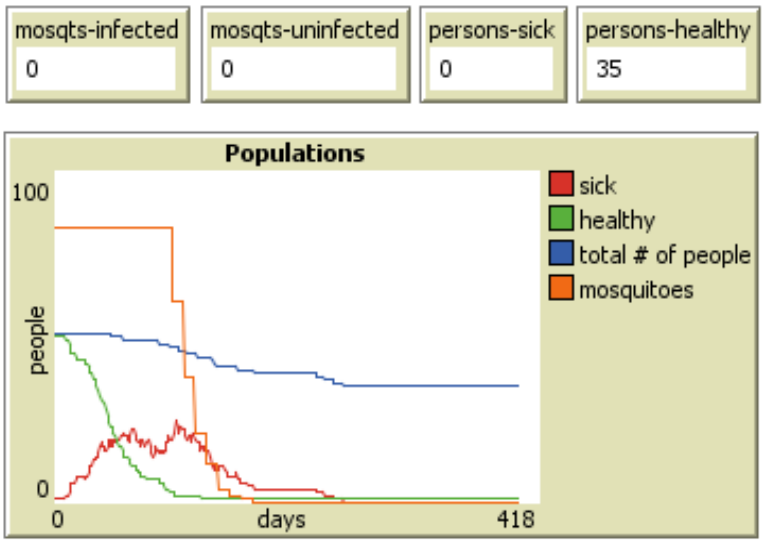

Fig. 6 Population graph plot with counts

Results show that the software is doing what it is programmed to do. Mosquitoes move about, bite, infect people and reproduce. People move about, some are immune, and the number days they have

been sick is recorded. They may get malaria when bitten by mosquitoes or die if they don't get treatment or recover after receiving treatment from clinics.

However, the simulation is very limited and many factors were not taken into consideration. A more complex model which integrates as many variables as possible to closely mimic real life actions of people can do a much better job at closely simulating the spread of malaria in a population. The model can be developed further to mimic day and night periods; instead of random movement once persons are infected they should be able to move towards a clinic; people should also spend more time within confined places like schools, homes and places of work instead of randomly moving around. These are all improvements which can be incorporated into the model.

Conclusion

The Malaria model aims to simulate the spread of Malaria in a human population; taking into account the various variables which perpetuate and hinder the spread of the disease with a view to understand how these variables influence the disease's perpetuation and/or prevention. Ecological biologists have suggested a number of factors which may influence the survival of a directly transmitted virus within a population [Yorke, et al.].

A model simulation thus greatly helps users gain a better understanding of the disease's epidemiology and to make plans for the corresponding prevention. This is therefore a tool which can be used by public health officials and disease epidemiologists to study disease perpetuation, and help create a better understanding

The Malaria model runs on NetLogo, a programmable modeling environment for simulating natural and social phenomena. NetLogo is touted to be particularly well suited for modeling complex systems developing over time. Modelers can give instructions to hundreds or thousands of 'agents' all operating independently. This makes it possible to explore the connection between the micro-level behavior of individuals and the macro-level patterns that emerge from their interaction [Wilensky]. NetLogo comes with many models to simulate various phenomena, ranging from Biology to Social Science giving one a head start as to how to apply or extend some of the already existing models or come up with new models. Among these default models; three are of interest to the Malaria model; which generally simulate the spread of diseases between agents and within populations with different variables which profoundly affect the spread of such diseases: a virus model, a disease-solo model and an HIV- Aids model.

Acknowledgements

Heartfelt thanks to Dr. Adem Ozyavas and Dr Bob Riggins for their support and advice in doing this project, both in and out of the classroom, their doors were always open and they've been of immense help. Furthermore, Thanks to Dr. Rodney Klein, Lisa Karnes and Vickie Hart from the McNair office at Concord University and all the people who conducted workshops on everything connected to getting into graduate school and beyond, you folks are a beacon of hope, the concern and attention you give to students is just truly admirable. Many thanks also to the other McNair scholars for a rewarding, educative and culturally enriching summer experience.

Works Cited

Organization, World Health. *World Malaria Report 2011*. Annual. Switzerland: WHO Press, 2011. Print.

Yorke, et al. "Seasonality and the requirements for perpetuation and eradication of viruses in populations." Journal of Epidemiology, volume 109, pages 103-123

Manvendra Narayan Mishra et al. "Mathematical Model to Simulate Infectious Disease." VSRD Technical & Non-Technical Journal, Vol. 3 (2), 2012, 60 - 68.

Wilensky, U. 1999.
NetLogo. http://ccl.northwestern.edu/netlogo/. Center for Connected Learning and Computer-Based Modeling, Northwestern University. Evanston, IL.

Wilensky, U. (1998). NetLogo Virus model. http://ccl.northwestern.edu/netlogo/models/Virus. Center for Connected Learning and Computer-Based Modeling, Northwestern University, Evanston, IL.

Wilensky, U. (2005). NetLogo Disease Solo model.
http://ccl.northwestern.edu/netlogo/models/DiseaseSolo. Center for Connected Learning and Computer-Based Modeling, Northwestern University, Evanston, IL.

Wilensky, U. (1997). NetLogo AIDS model. http://ccl.northwestern.edu/netlogo/models/AIDS. Center for Connected Learning and Computer-Based Modeling, Northwestern University, Evanston, IL.

Christoph Aschwanden, "Spatial Simulation Model for Infectious Viral Diseases with Focus on SARS and the Common Flu," hicss, vol. 6, pp.60137b, Proceedings of the 37th Annual Hawaii International Conference on System Sciences (HICSS'04) - Track 6, 2004

NetLogo Online Community

Hemlock Establishment and Vigor in Twin Falls Resort State Park, West Virginia

Mary Elizabeth Ryan

Dr. Tom Saladyga

Abstract

Eastern hemlock (*Tsuga canadensis* L.) is a coniferous tree that ranges through the north and eastern parts of the United States and into neighboring Canada. Hemlock wooly adelgid, an exotic insect that was introduced to the United States from Japan, feeds on the sugar in the hemlock tree's needles, which is causing a rapid decline in eastern hemlock. We established six long-term monitoring plots in the summer of 2013 in Twin Falls Resort State Park, located in Wyoming County, West Virginia. All trees ≥ 10 cm *diameter at breast height* (DBH) were tagged and measured within each 707 m^2 (0.07 ha) plot. All hemlock trees were assigned a vigor ranking from 1 (healthy) to 5 (functionally dead). A subsample of hemlock was cored to determine temporal patterns in hemlock establishment. Of the total trees sampled (live and dead) the results of the study show that the IV of hemlock was higher by far than any other tree species encountered within the plots. Results indicate that 98% of 177 hemlock trees are either in decline or functionally dead. The majority of hemlock established was during the 1920s and 1930s, while the earliest inner ring date was 1815. More research must be conducted in order to further our understanding of the regional impacts of HWA on hemlock forest systems.

Introduction

Eastern hemlock (*Tsuga canadensis* L.) can be found throughout New England and south through New York and Pennsylvania. Hemlock also grows in the Middle Atlantic States, from New Jersey west to the Appalachian Mountains, and south to Georgia and Alabama (Godman and Lancaster 1990). Hemlock is predominately found growing in low light conditions with minimal temperature change (Rogers 1980; Canham et al. 1994). Hemlock thrives in north- and east-facing slopes and in environments where there is high humidity and cool temperatures (Benzinger 1994a, b, c). It has shallow roots, which increases its sensitivity to extreme conditions such as drought or high amounts of water, which can be fatal (Graham 1943; McIntyre and Schnur 1936; Secrest et al. 1941; Stickel 1933). Wildlife is dependent on the canopy of hemlock forests, which keep streams at temperatures suitable for aquatic life (Ward et al. 2004). There was a decline of eastern hemlock 5,800 years ago due to climate changes and pathogens that lasted 1,000 years (Haas and McAndrews 2000). In the past 100 years, the structure and composition of northeastern forests have been changing due to the introduction of exotic insects and pathogens, such as chestnut blight, emerald ash borer, and hemlock wooly adelgid (HWA) (Small et al. 2005).

Hemlock wooly adelgid is an exotic insect that was introduced to the United States from Japan (Eschtruth et al. 2006). These insects feed on the ray parenchyma cells that are in the tree's needles (Young et al. 1995), which has resulted in rapid hemlock decline and increased mortality rates. HWA was first documented in the eastern U.S. in 1951 (Spaulding and Rieske 2010) and was found in West Virginia and Virginia in the 1950's (McClure 1987). Since the infestation has occurred, there have been major impacts on hemlock forest systems. These infested trees usually have a slim chance of recovery (Kizlinski et al. 2002). HWA also reduces the production of new seeds causing lower rates of regeneration (Orwig and Foster 1998). Studies conducted in southern Ontario, Canada have shown that the mortality of hemlock is causing other species to have an increase in pollen from tree taxa and an increase in pollen influx values (Fuller 1998).

The decline of hemlock is also impacting birds that depend on the tree species for nesting. Hemlock has lower branches than most conifers and gives birds more space for nesting and feeding (Haapanen 1965). Research has shown that there are higher amounts of birds nesting in hemlock forests that are not affected by HWA as compared to sites that are (Becker et al. 2008). These results indicate that birds have to find new nesting and feeding sites when HWA infestation causes hemlock mortality. The decline is also affecting stream temperatures which negatively impacts aquatic life. Needle decay occurs when the HWA eat the sugar from the base of hemlock needles, resulting in canopy loss and decreased shade. With less shade there will be an increase in stream water temperature which negatively impacts fish populations (Onken 1995).

The decline of hemlock due to HWA is being monitored in varies areas. Long-term monitoring was introduced in 1990-1991to Shenandoah National Park, Virginia. During the monitoring period, mortality has increased and crown health has declined (Bair 2002). In northeastern Pennsylvania in the Delaware Water Gap National Recreation Area, there has been a study on HWA effects on forest health. This was the first study to use pre-infestation data in order to monitor forest response to HWA over a nine year period. The study indicated that hemlock decline will cause changes in vegetation, increased inputs of coarse woody debris, and will result in hardwood trees replacing hemlock in many areas (Eschtruth et al. 2006). Forest Vegetation Simulator (FVS) models have been developed to predict changes in hemlock forests in the southern Appalachians and Cumberland Plateau. Models were made showing what hemlock forests would be like after 20 years with HWA infestation (Spaulding and Rieske 2010). The models indicate that hemlock forests without HWA would have little change, but forests with HWA would experience near 100% mortality. The results also show that the decline will cause an increase in hardwood trees that will create canopy gaps. These canopy gasps will let exotic plants grow, changing the vegetation and affecting the habitats of wildlife species (Spaulding and Rieske 2010).

In West Virginia, forest monitoring is being conducted by the Eastern Rivers and Mountains Network (ERMN) to assess long-term ecosystem dynamics. Vegetation and soil is being monitored at

New River, Bluestone, and Gauley National Scenic Rivers (NPS/ERMN/NRR 2010). Monitoring was also set up in Cathedral State Park in Preston County, WV in 1965 and has been checked in 2000 and 2006 to document the effects of HWA (Beane et al. 2010). The WV Department of Agriculture has a plan to manage the infestation of HWA using annual plot monitoring in Cathedral State Park, Greenland Gap, and Blackwater Falls. They released beetles onto sites that are monitored every season once a month for four months in order to learn the effects of the beetles on HWA. Imidacloprid chemical injections have also been used to treat 1,400 trees. The injections are successful for individual trees and are designed to cause the insect's nervous system to fail, with minimal effects to other insects or mammals (WVDA 2007).

Many scientists have used dendroecology and other methods to study the effects of HWA due to these vast changes in forest systems. Foster and others (2006) have studied climate change in relation to HWA and have found increased pollen from tree taxa in the 17 sites they studied across southern New England. The results indicated that the decline in this area was affected by dry conditions in the mid-Holocene period. Studies have also been done to see how HWA will impact the carbon cycle. It was discovered that high input of detritus from hemlock decline will result in a rapid influx of carbon in forest soils. It was also found that *Rhododendron maximum* will replace hemlock causing higher soil carbon (Nuckolls et al. 2009).

Studies on the relationship between elevation and HWA have concluded that lower elevations have higher rates of hemlock decline possibly due to temperatures being higher and precipitation being lower (Bair 2002). Beane and others (2010) have concluded that canopy gaps from hemlock decline will result in increased regeneration of shade intolerant species. Hemlock species that survive HWA will be out competed in areas of high hemlock mortality. In a two year study in north-central Massachusetts, results showed that deciduous species that replace hemlock will use higher amounts of water than hemlock-dominated forests (Hadley et al. 2008). The objective of this research was to establish baseline conditions of eastern hemlock forests in Twin Falls Resort State Park in southern West Virginia. Long-

term monitoring will be important for understanding the impacts of HWA on forest composition, structure, and ecosystem function.

Methods

Study Area

Research was conducted in the summer of 2013 in Twin Falls Resort State Park, located in Wyoming County, southwest of Beckley, West Virginia. The site's highest elevation is 750 m and its lowest elevation is 510 m (National Elevation Dataset 2002). Two waterfalls can be found on the site, which are a part of the extreme upper border of the Mississippi River watershed. The park is 3,776 acres large (Twin Falls Resort 2013). Statewide the average temperature of WV is 11°C (Law and Mogil 2011). Six plots have been established, three on Jackson Branch and three on Dixon Branch (Figure 1). The plots were located on north-facing slopes, where hemlock usually dominates. Jackson Branch plots are in areas untreated for HWA and Dixon Branch plots are in treated areas where the effects of the treatments can be monitored.

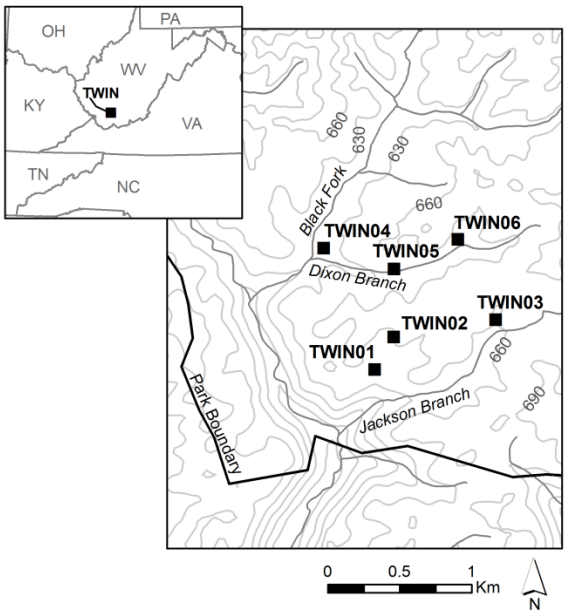

Figure 1 Map of six long-term monitoring plots along Dixon and Jackson Branch at Twin Falls Resort State Park, West Virginia.

Field Methods

Long-term monitoring plots were established using methods designed by the National Park Service's Eastern Rivers and Mountains Network (NPS/ERMN/NRR 2010). Geographic coordinates of plot centers, elevation, aspect, slope, and terrain position were recorded for each 15 m radius plot. The total plot area was 707 m^2 (0.07 ha) and all trees ≥ 10 cm *diameter at breast height* (DBH) were marked by a nail and a numbered aluminum tag. Tree species, DBH, life status, crown position, presence of pests/pathogens, and vigor were all recorded. Tree vigor was measured by a ranking system of healthy (<10% missing/damaged crown), light decline (<25% missing/damaged crown), moderate decline (26-50% missing/damaged/dead crown), severe decline (>50% missing/damaged crown), and functionally dead (mostly all crown missing/dead) (NPS/ERMN/NRR 2010). The importance values (IV) of the trees were calculated (IV = relative frequency/relative basal area)/2).

Lab Methods and Analysis

Hemlock stand age at each plot was determined by using standard dendrochronology methods (e.g. Stokes and Smiley 1968). Two cores were taken from each tree 10 cm above ground from healthy and standing dead with DBH ≥ 10 cm (trees=33). Samples were mounted on wood core mounts then sanded with progressively finer grit sandpaper for better visibility of cells. Each sample was scanned at 3,200 dpi using a high resolution flatbed scanner. Digital images of each core sample were loaded into the image analysis program CooRecorder (Larsson 2003), which was used to measure the rings of each sample. The samples were crossdated using the program CDendro 7.6. in order to establish accurate inner ring dates for each tree. Inner ring dates were binned into 10 year increments to summarize dates.

Results

Of the total trees sampled (live and dead) the results of the study show that hemlock is an important species to the park, as indicated by an IV > 0.5 (Figure 2). This IV is greater by far than any other tree species encountered within the plots. The other species found to have high importance in the

park were tulip poplar, sweet birch, and red maple. Eastern hemlock's IV is more than of all the other species found within the plots combined.

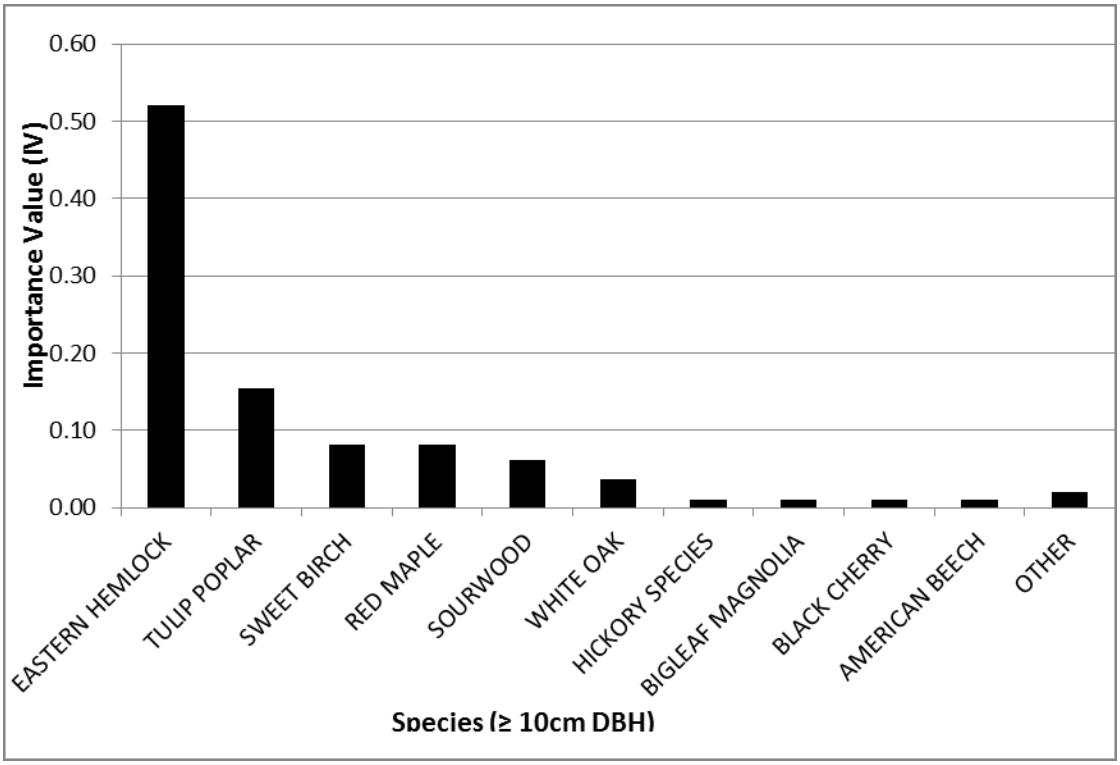

Figure 2 Importance values of tree species (live and dead) found in plots whose DBH was ≥ 10cm. [IV= (relative frequency/relative basal area)/2] Other trees whose IV was < 0.1, included red oak, black oak, black gum, and unknown species (decayed snags).

The results of the vigor assessment indicate that most of the hemlock within Twin Falls is in decline (Figure 3). Results show that 98% of the 177 hemlock trees are in decline or functionally dead. Fifty percent of the 177 eastern hemlock trees that were sampled are in moderate decline.

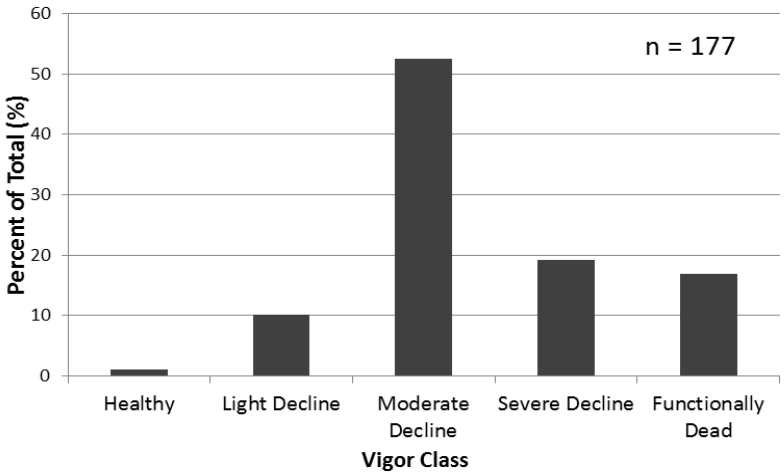

Figure 3 Percent decline of 177 eastern hemlock trees sampled, shown by vigor class.

The results of the age structure analysis for a sub-sample of hemlock trees showed that 17 of the 33 trees had an inner ring date during the 1920s and 1930s (Figure 4). From the sub sample, only one tree was dead with an inner ring date of 1932**.** The earliest inner ring date was 1815 and the latest was 1947. The distribution of inner ring dates suggests that forest disturbance during the late 19th and early 20th Centuries encouraged hemlock establishment during the 1920s and 1930s.

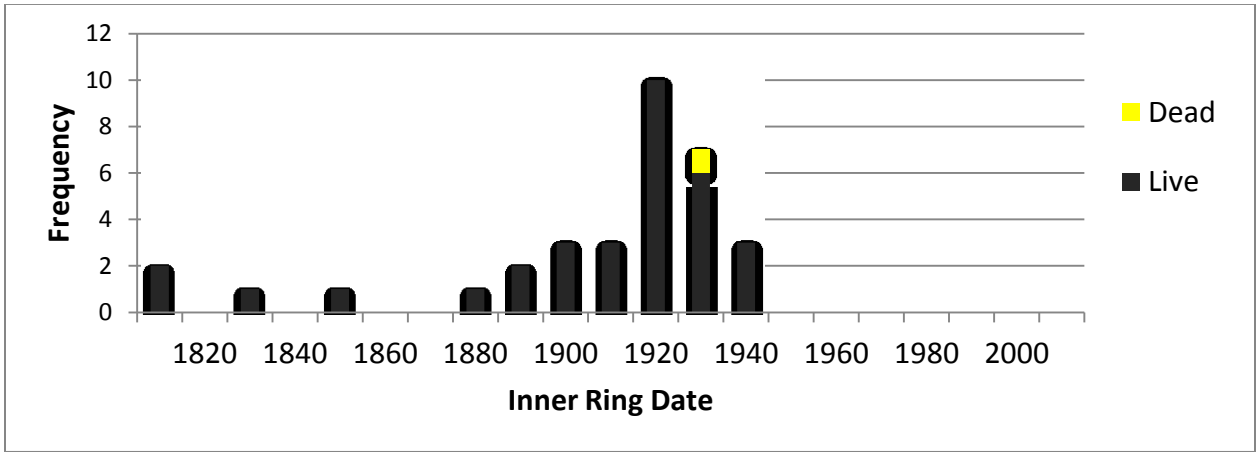

Figure 4 Age structure distribution of inner ring dates from a sub-sample of 33 hemlock trees. Black represents live trees and yellow represents dead trees.

Discussion

Our results indicate that eastern hemlock at Twin Falls Resort State Park is in a decline, which will likely continue into the near future. This result is similar to Shenandoah National Park, Virginia where an increase in the mortality of eastern hemlock was observed from 1999 to 2001 (Bair 2002). In a study in southern New England, 7 of 8 hemlock stands had over half of the hemlock in vigor class 4 (1-25% foliage) and 5 (dead) (Orwig and Foster 1998). Hemlock at Twin Falls is experiencing a moderate decline at the present time and will likely increase in mortality over the years as HWA spreads from east to west. Unlike in these forests, in Cathedral State Park HWA was found to have little or no impact on the overstory, understory, basal area, or volume of the hemlock trees (Beane et al. 2010). This observation suggests that different forest structures (i.e. old growth vs. second growth) are reacting differently to HWA infestation.

The trees that made up the highest amount of the plots at Twin Falls were hemlock followed by tulip poplar, sweet birch, and red maple. In Cathedral State Park, hemlock was the most frequent overstory species encountered in the park at 59% in 2000 and 61% in 2006. Additional species were red maple at 13% and 11%, sweet birch at 11% and 10%, and black cherry at 6%, while the other species made up less than 4%. Hemlock also dominated in basal area and in the understory with red maple and black cherry close behind (Beane et al. 2010). These results are very similar to that of Twin Falls, yet Cathedral, with its old growth hemlock, has a different age structure of forest than that of Twin Falls. Of the 982 trees observed at Cathedral State Park, 12% were infested, and two of the plots were 90% infested with HWA (Beane et al. 2010).

The reason for the increase of hemlock during the 1920's is most likely do to the large amount of logging that occurred in Wyoming County during the previous decades. Major logging starting taking place in 1889 when logs where being floated down the Guyandotte River to the Ohio River in Huntington, WV (e-WV 2013). The logs were used to build cabins, barns, sheds and for other purposes that factored in the further settlement of the region (Blankenship 2011). The inner ring dates of the

hemlock trees in Twin Falls indicate that this was what was happening from the 1880's to the early 1900's. The logging removed many mature trees from the forest and contributed to hemlock recruitment, especially in the 1920's.

While logging disturbance encouraged the recruitment of hemlock at Twin Falls during the early 20th century, New England is experiencing the effects of logging today. In Connecticut a total of 2410 ha of the hemlock forest was lost to logging in the last 6 years (Orwig and Foster 1998). When combined, the effects of HWA, logging, and development caused 30% of the area that was mapped as hemlock in 1980 to now be different land cover types. More than half of the hemlock cover in an 1880 ha forest tract was lost due to HWA-induced mortality. A total of 4290 ha of forest was lost due to logging and HWA since the 1980's in the southern portion of a research transect. In 1998 it was predicted that hemlock mortality will continue to increase in the northeastern U.S. (Orwig and Foster 1998).

Conclusion

It is most likely that HWA effects will continue to increase as HWA spreads and moves into unaffected areas. The hemlock trees that are at a moderate decline now may be in a severe decline within the next decade or earlier. Solutions today can only help on a small level and cannot help large scale forests. More research will have to be conducted in future years to document the continued effects of HWA on the hemlock forests in Twin Falls Resort State Park. Monitoring networks can be established in order to share results as a way to further our understanding of the regional impacts of HWA on hemlock forest systems.

References Cited

Bair, Mary Willeford. "Eastern hemlock (Tsuga canadensis) mortality in Shenandoah National Park." *Proceedings, Hemlock woolly adelgid in the Eastern United States symposium*. 2002.

Beane, Nathan R., Eric Heitzman, and Thomas M. Schuler. "Stand dynamics of an old-growth eastern hemlock-hardwood forest in West Virginia." *Natural Areas Journal* 30.1 (2010): 64-72.

Becker, Douglas A., Margaret C. Brittingham, and Christopher B. Goguen. "Effects of hemlock woolly adelgid on breeding birds at Fort Indiantown Gap, Pennsylvania." *Northeastern Naturalist* 15.2 (2008): 227-240.

Benzinger, J. "Hemlock decline and breeding birds. I. Hemlock ecology." *Records of New Jersey Birds* 20.1 (1994): 2-12.

Blankenship, Paul Ray. " Logging became natural endeavor to pioneers » History of Wyoming County » Wyoming County Report." *Home Page » Wyoming County Report* . N.p., n.d. Web. 12 Sept. 2013. <http://www.wycoreport.com/wycohistory/x449324926/Logging-became-natural-endeavor-to-pioneers>.

Canham, Charles D., et al. "Causes and consequences of resource heterogeneity in forests: interspecific variation in light transmission by canopy trees." *Canadian Journal of Forest Research* 24.2 (1994): 337-349.

Department of the Interior, National Park Service, Eastern Rivers and Mountains Network. (2010*). Vegetation and soil monitoring protocol for the Eastern Rivers and Mountains Network, Version* 2. Natural Resources Report: NPS/ERMN/NRR 2010.

Eschtruth, Anne K., et al. "Vegetation dynamics in declining eastern hemlock stands: 9 years of forest response to hemlock woolly adelgid infestation." *Canadian Journal of Forest Research* 36.6 (2006): 1435-1450.

"e-WV | Wyoming County." *e-WV | The West Virginia Encyclopedia*. N.p., n.d. Web. 12 Sept. 2013. <http://www.wvencyclopedia.org/articles/1381>

Foster, David R., et al. "A climatic driver for abrupt mid-Holocene vegetation dynamics and the hemlock decline in New England." *Ecology* 87.12 (2006): 2959-2966.

Fuller, Janice L. "Ecological impact of the mid-Holocene hemlock decline in southern Ontario, Canada." *Ecology* 79.7 (1998): 2337-2351.

Godman, R. M., and Kenneth Lancaster. "Tsuga canadensis (L.) Carr. eastern hemlock." *Silvics of North America* 1 (1990): 604-612.

Graham, Samuel Alexander. *Causes of hemlock mortality in northern Michigan*. University of Michigan Press, 1943.

Haapanen, Antti. *Bird fauna of the Finnish forests in relation to forest succession: I*. Diss. Suomalaisen Kirjallisuuden Kirjapaino, 1965.

Haas, J. N., & McAndrews, J. H. (2000). The summer drought related hemlock (Tsuga canadensis) decline in Eastern North America 5700 to 5100 years ago. In *K. McManus, editor Proceedings. Symposium on Sustainable Management of Hemlock Ecosystems in Eastern North America (Durham, New Hampshire, USA, 1999). USDA Forest Service General Technical Report NE-267* (pp. 81-88).

Hadley, Julian L., et al. "Water use and carbon exchange of red oak-and eastern hemlock-dominated forests in the northeastern USA: implications for ecosystem-level effects of hemlock woolly adelgid." *Tree Physiology* 28.4 (2008): 615-627.

Kizlinski, Matthew L., et al. "Direct and indirect ecosystem consequences of an invasive pest on forests dominated by eastern hemlock." *Journal of Biogeography* 29.10-11 (2002): 1489-1503.

Larsson, L. A. "CooRecorder: image co-ordinate recording program." *Cybis Elektronik & Data AB, Saltsjöbaden, Sweden* (2003).

Law, Kevin T., and H. Michael Mogil. "Weatherwise Magazine -- March-April 2011." *Weatherwise Magazine -- September-October 2013*. N.p., n.d. Web. 21 Aug. 2013. <http://www.weatherwise.org/Archives/Back%20Issues/2011/March-April%202011/west-virginia-full.html>.

McCLURE, MARK S. *Biology and control of hemlock wooly adelgid*. Vol. 851. Bulletin 851: Connecticut Agricultural Experiment Station, 1987.

McIntyre, Arthur Clifton, and G. Luther Schnur. "Effects of drought on oak forests." The Pennsylvania State College, School of Agriculture and Experiment Station. (1936).

Nuckolls, April E., et al. "Hemlock declines rapidly with hemlock woolly adelgid infestation: impacts on the carbon cycle of southern Appalachian forests." *Ecosystems* 12.2 (2009): 179-190.

Onken, Bradley P. "Long-term impact assessment of eastern hemlock forests." *Proceedings of the first hemlock woolly adelgid review, Charlottesville, VA* (1995): 96-10.

Orwig, David A., and David R. Foster. "Forest response to the introduced hemlock woolly adelgid in southern New England, USA." *Journal of the Torrey Botanical Society* (1998): 60-73.

Rogers, Robert S. "Hemlock stands from Wisconsin to Nova Scotia: transitions in understory composition along a floristic gradient." *Ecology* (1980): 178-193.

Secrest, H. C., H. J. MacAloney, and R. C. Lorenz. "Causes of the decadence of hemlock at the Menominee Indian Reservation, Wisconsin." *Journal of Forestry* 39.1 (1941): 3-12.

Small, Melanie J., Christine J. Small, and Glenn D. Dreyer. "Changes in a hemlock-dominated forest following woolly adelgid infestation in southern New England 1." *The Journal of the Torrey Botanical Society* 132.3 (2005): 458-470.

Stickel, Paul W. "Drought injury in hemlock-hardwood stands in Connecticut." *Journal of Forestry* 31.5 (1933): 573-577.

Stokes, Marvin A. *An introduction to tree-ring dating*. University of Arizona Press, 1996.

Spaulding, Heather L., and Lynne K. Rieske. "The aftermath of an invasion: structure and composition of Central Appalachian hemlock forests following establishment of the hemlock woolly adelgid, Adelges tsugae." *Biological Invasions* 12.9 (2010): 3135-3143.

"Twin Falls Resort State Park." *Twin Falls Resort State Park*. N.p., n.d. Web. 21 Aug. 2013. <http://www.twinfallsresort.com/faqs.html>

United States Geological Survey. National Elevation Dataset. (2002).

Ward, Jeffrey S., et al. *Eastern hemlock forests: guidelines to minimize the impacts of hemlock woolly adelgid*. Vol. 4. No. 3. Connecticut Agricultural Experiment Station, 2004.

West Virginia Division of Agriculture, Cooperative Forest Health Protection Program. *Hemlock Woolly Adelgid Management Plan*. (2007).

Young, Rebecca F., Kathleen S. Shields, and Graeme P. Berlyn. "Hemlock woolly adelgid (Homoptera: Adelgidae): stylet bundle insertion and feeding sites." *Annals of the Entomological Society of America* 88.6 (1995): 827-835.

THE SIGNIFICANCE OF BLOOD VISCOSITY ON BLOODSTAIN

PATTERN ANALYSIS

By

Cynthia White

A research paper

Submitted in Partial Fullfilment of the Requirements for the

Bachelor of Science in Applied Science Degree

Department of Arts and Sciences in the undergraduate school

Bluefield State College

April 2014

Graduation Date: May 2014

Abstract:

Bloodstain Pattern Analysis (BPA) is a technique used to investigate scenes of violent crime and death. BPA uses physics, math and statistics to interpret the size, shape, and pattern of the blood shed during an act of violence. Viscosity and surface tension are important factors in the formation of liquid drops and thus may significantly affect the statistical properties of bloodstain patterns. The goal of this study was to determine whether different blood viscosities create measurably different bloodstain patterns. It was thought lower blood viscosities would yield smaller droplets at higher quantities and would reach farther distances. It was important to have synthetic blood emulating the viscoelastic and electrical properties of real blood so the impact patterns would closely simulate that of a violent scene. Impact spatter patterns were created using synthetic blood that was made by using a formula found in *Evaluation of a transparent blood analog fluid Aqueous Xanthan gum/glycerin*[1]. Five viscosities of synthetic blood were manufactured. The impact spatter patterns were created using a unique apparatus constructed in the lab. Blood droplets were characterized by shape and radial distance from the point of impact and counted. Counts were compared across the five viscosities. The statistical power of the sample size was insufficient to produce any discernible trend correlated to viscosity. Increasing the statistical power by decreasing the number of viscosities and performing more trials at each viscosity may yet yield statistically significant results.

Introduction:

The Centers for Disease Control and Prevention (CDC) report that for the years 2000 to 2010, homicide in the United States ranked, for eight of the eleven years, number five of the ten leading causes of death in Americans ages 25-44, of all races and both sexes[2] (Table 1). This statistical information suggests homicide has been a steady problem within the United States for a long time.

Year	Rank
2010	5
2009	5
2008	No Data
2007	5
2006	5
2005	5
2004	3
2003	5
2002	5
2001	5
2000	6

Table 1:Rank of homicide among the 10 leading causes of death in Americans aged 25-44 of all races and both sexes.

Bloodstains are the type of physical evidence most frequently encountered at scenes of violence. The analysis of those bloodstains, termed Bloodstain Pattern Analysis (BPA), is the tool utilized most in the reconstruction and interpretation of scenes of violent crime and death[3].

While the interpretation of bloodstains left at crime scenes has probably occurred on some level throughout human history, the first recorded attempt to systematically apply scientific methods and reasoning to BPA occurred in 1895 when Polish criminologist Dr. Eduard Piotrowski published *Uber Entstehung, Form, Richtung and Ausbreitung der Blutspeuren nach Niebwunden des Kopfes* (*Concerning Origin, Shape, Direction and Distribution of the Bloodstains following head Wounds Caused by Blows*)[4]. The first time that BPA was upheld as a valid form of evidence in the United States criminal court system was in 1955 in the case of *The State of Ohio vs. Samuel Sheppard.*[5] Today, BPA uses physics, math and statistics to interpret the size, shape, and pattern of the blood shed during an act of violence. BPA evidence is now regularly used to distinguish between suicide and homicide[6,7], establish the distance between shooter and victim[8], and predict the location of the victim at the time of injury[9].

The bulk of the scholarly work on BPA has been directed toward techniques for determining Area of Origin (AO) from bloodstains. The general idea behind locating AO is to look at a blood droplet, determine at what angle it hit the surface (angle of impact) and extend that line of impact into space until it intersects with other lines of impact. The volume of space in which the impact lines intersect is the AO.

In the traditional method, this process is accomplished by a technique called stringing. The angle of impact is determined, and a string is stretched from the drop across the room where it is anchored with a place holder. This is repeated for several blood droplets. Once there are a sufficient amount of strings, they are examined. The point at which the strings cross is the AO and the presumed location of the victim at the time of injury. This method does not take into consideration gravity and its effect on the blood droplets' flight[10].

Increasingly, this analysis is done with computers. High resolution images are taken of the crime scene

and uploaded into a computer. The computer selects droplets, calculates the angle of impact and visualizes the trajectory. These programs can include physics models to take into account gravitational and air resistance effects.

Very few studies have been conducted on how abnormal conditions can affect bloodstain patterns. Hemocrit levels, for example, have been shown to affect the elastic properties of blood[11], but the effect of hemocrit levels, which could be measured from blood swabs at a crime scene, on bloodstain patterns has not been studied.

Since inebriation is a factor in a minimum of 40% of homicides in the U.S[12], how the presence of drugs and alcohol in the blood affects bloodstain patterns is of particular interest. A study evaluating the effects of the blood-thinner warfarin on bloodstain patterns[13] found that an increase in warfarin lead to a decrease in the viscosity of the blood, which in turn resulted in variation of the determined final diameter of the bloodstain patterns.

While warfarin's main use is to reduce blood viscosity, increased Blood Alcohol Content (BAC) is associated with increased blood viscosity[14]. The original intent of this research was to analyze whether BAC has a significant effect on bloodstain patterns. Experimental design considerations, including the lack of readily available blood samples with varying BAC, led to the formulation of the current project, which attempts to identify statistical differences in the impact patterns (which are produced when an object strikes liquid blood on a surface or another object[15]) formed by different viscosities of synthetic blood.

Liquids flow and drip differently according to their viscosity[16]. Viscosity, which arises from internal forces of a fluid, determines the ease at which that fluid can flow[17]. The behavior of the liquid depends on whether it is Newtonian or non Newtonian. Newtonian fluids have a linear relationship between the amount of force (shearing stress) acting on the fluid and the fluid's deformation.

Non-Newtonian fluids respond non-linearly to increasing shearing stress (Figure 1). The harder the force that acts on the non-Newtonian fluid, the higher or lower the flow resistance. Some examples of Newtonian fluids are water, juice, and milk: no matter how hard you hit it, the flow resistance remains the same. One example of a non-Newtonian fluid is cornstarch

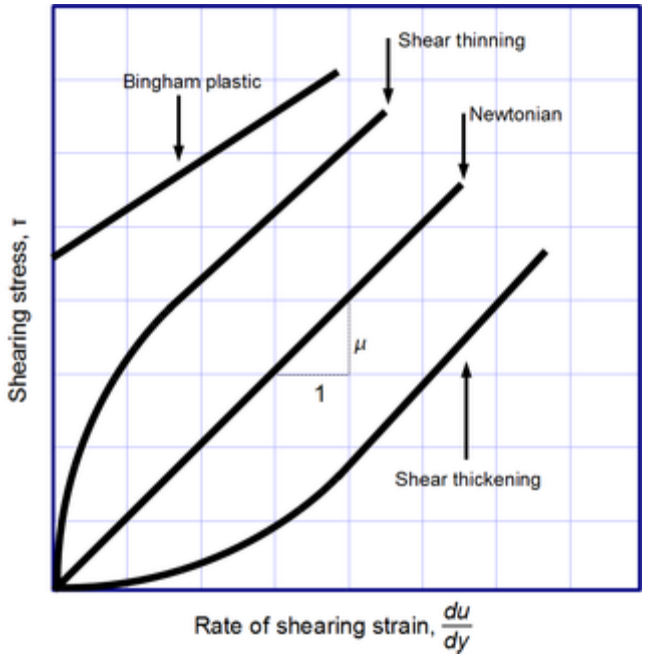

Figure 6: In this shearing stress vs shearing strain plot, the viscosity is the slope of the curve. Newtonian fluids exhibit no change in viscosity relative to applied force. Shear thickening and shear thinning fluids increase and decrease in viscosity, respectively, with increased force. Bingham plastics behave as a solid below some threshold, then act as a Newtonian fluid.

mixed with water. The more cornstarch is added, the more non-Newtonian it becomes. When one slowly pushes into the mixture it acts like a liquid, but when struck it acts like a solid. Blood is a non-Newtonian fluid[18].

According to Peschel, Kunz, Rothschild, and Mützel, blood makes up approximately 8% of the body weight. The average density of blood is approximately 1,060 kg/m^3. The average adult has from about 4–5 L (female) and up to 5–6 L (male) of blood[19].

Because viscosity affects droplet formation[20], it is important to have a blood substitute with the same viscous properties of blood. Brookshire and Tarbell developed a formula of xanthan gum, glycerin, and sodium chloride (NaCl) that accurately models the viscous, surface tension, and electrical conductivity properties of blood[1]. Altering the glycerin to water ratio will increase or decrease the viscous component without manipulating the elasticity[10]. The NaCl is used to emulate the electrical conductivity of blood.

Hypothesis

Higher viscosity blood is expected to produce patterns with fewer, larger droplets located nearer the source.

Materials and methods

Synthetic Blood

Five different viscosities (Table 2) of synthetic blood were manufactured based on a formula by Brookshire and Tarbell[1]. Distilled water and sodium chloride (NaCl) in the formula replicate the electrical properties of blood. Glycerin modulates the viscosity of the mixture. Xantham gum is used to emulate surface-tension. In this experiment, red food color was added as a part of the water to produce a pattern more readily visible on the white butcher paper. The xantham gum was eliminated because it obstructed the capillary tube in the viscometer.

Label	Water (g)	NaCl (g)	Glycerin (g)	Average η (mm^2/s)
V1	55.500	0.500	25.000	2.3
V2	55.500	0.500	30.000	2.7
V3	55.500	0.500	40.000	3.6
V4	55.500	0.500	46.500	4.1
V5	55.500	0.500	49.000	4.6

Table 2: Synthetic blood formulations. The listed amount of water includes red food coloring. The volume of water and salt base was kept constant while the glycerin content was varied. Viscosity V_3 was mixed according to the proportions listed in Brookshire and Tarbell to replicate the average viscosity of human blood of 3-4 mm^2/s.

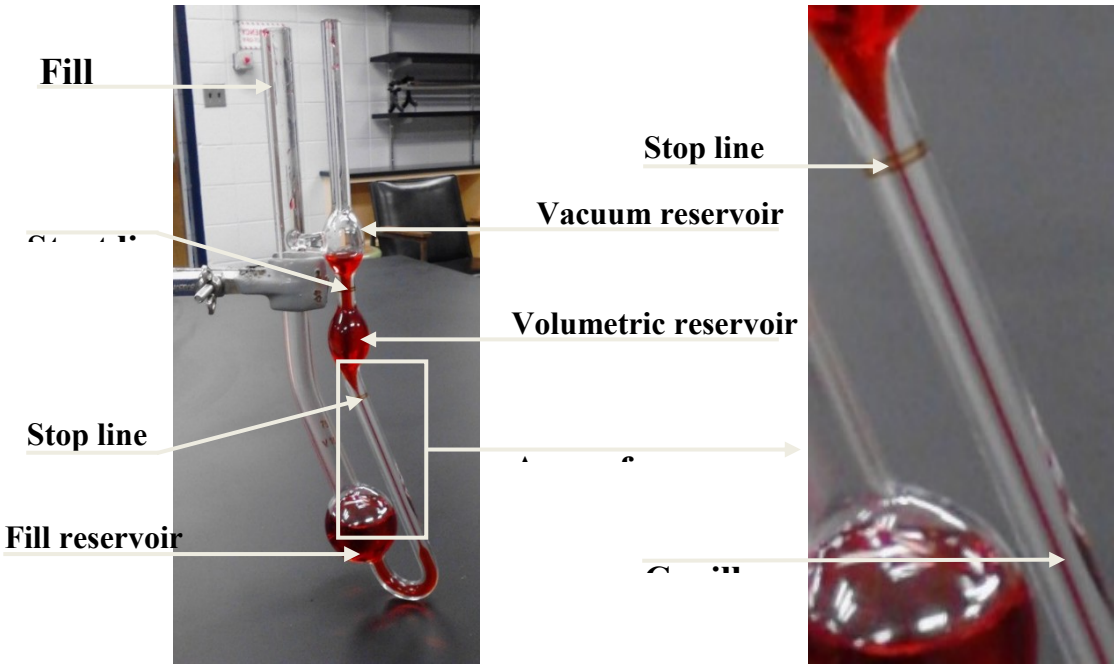

Figure 7: Cannon-Fenske Routine viscometer. The time it takes a specified volume V, to flow through the capillary is used to calculate the viscosity η. The fluid is poured into the fill tube and drawn into into the vacuum reservoir on the vacuum tube by a vacuum. The vacuum is released and a timer is started and stopped when the meniscus passes the start and stop lines.

Viscosities were measured using a Cannon-Fenske Routine viscometer (Cannon Instrument Company PN: V15) (Figure 2) according to the manufacturer instructions, where the output variable was the time (t) it took a specified volume (6.2 mL) of fluid to traverse the capillary.

The viscosity was calculated using the equation

$$n = tC\Delta T$$

where η is the viscosity of the fluid, t is the time it takes for the fluid to flow through the capillary tube, C is the constant given by the manufacturer, and ΔT is the change in temperature of the fluid from the callibration temperature.

Impact-Pattern Apparatus

Initial Design

The original design of the impact-pattern apparatus is illustrated in (Figure 3) . An electromagnet was set to a specific height using a lab upright and crossbar. The electromagnet was used to hold a

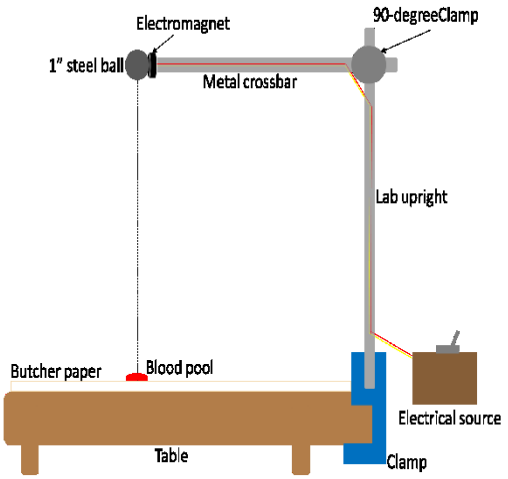

Figure 8: This spatter pattern apparatus was made of a lab upright to give height to the metal crossbar that anchored the electromagnet. A 1" steel ball was held by the electromagnet through magnetic forces controlled with an electrical source. Switching the electrical source to the off position allowed the ball to be released into a free fall to make impact with the pool of blood below on a piece of

1”-steel ball. A pool of synthetic blood was placed on the butcher paper directly beneath the steel ball, which was then released by cutting of the electrical supply to the electromagnet. This design was ultimately rejected because (1) the paper tended to absorb and wick the blood before impact (2) the steel ball did not land consistently in the center of the pool (3) the blood tended to spread rather than spatter (4) the steel ball would bounce producing secondary marks.

Final Design

The initial design was modified as in (Figure 4). A plastic bottle cap was placed inside-down on the paper and a string was suspended from the metal crossbar, strung through a 1” steel ball and the bottle cap and secured to a piece of cardboard.

The bottle cap served two purposes: to prohibit the blood from soaking into the paper, and to give the blood pool elevation so the droplets could have some vertical movement as well as a longer flight horizontally before making contact with the paper. This was to ensure the formation would simulate bloodstain patterns investigators encounter when investigating violent scenes.

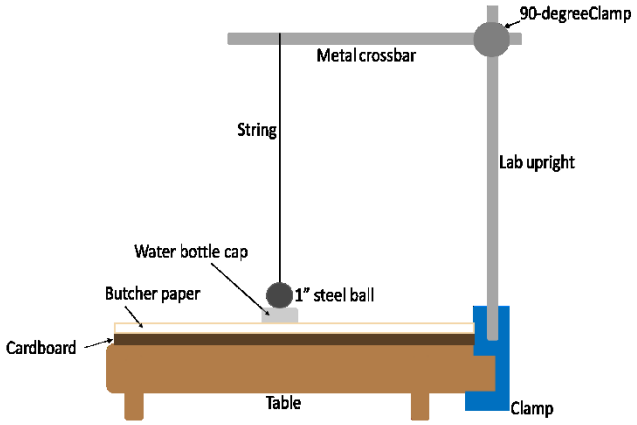

Figure 9: The spatter pattern apparatus shown here is representative of the one used for this project. Here a lab upright gives height to the metal crossbar anchoring the string that is anchored on the other end by a sheet of cardboard. Also threaded onto the string is a 1” steel ball used for impact on the ball and a water bottle cap used to prevent absorbtion of the blood into the paper and to give elevation to the pool of blood.

The force with which the blood pool was impacted remained constant by raising the ball all the way to the crossbar every time.

The equation of kinematics

$$v_f^2 = v_i^2 - 2gh$$

indicates that if objects are dropped with the same initial velocity v_i (in this case zero) from the same height h, they will hit with the same velocity v_f because g is the gravitational field which is a constant $9.8\frac{\mathrm{m}}{\mathrm{s}^2}$ near the surface of the earth. This is true for different objects or the same object dropped repeatedly. Thus the ball is known to reach the bottle cap with a velocity of v_f every trial. The collision itself is governed by the impulse-momentum theorem, which states that for a constant force F, and constant mass m

$$F \cdot t = m\left(v_f - v_i\right)$$

where t is the time over which the impact occurs. While there are always underlying random variations in any sufficiently complex real process, there is no reason to believe that t changes in a significant way in this experiment. Thus solving for F yeilds

$$F = m\left(\frac{\Delta v}{t}\right)$$

which is an expression of Newton's second law more commonly written

$$F = ma^{20}$$

Measurements:

Each pattern had 4 radii drawn on them with a drawing compass (Figure 5).

Inside each radius and outside the 13cm radius 3 types of drops were measured. Droplets that were mostly circular were called "spherical", elongated ones were called "prolate", and the ones that could not easily be catagorized by either one of the previous were called "irregular". Each type of drop was divided into 3 sizes; <2cm, 2-5cm, and >5cm.

Results

(Table 3) summarizes the measurements taken and calculations made to measure the viscosity for the five samples of synthetic blood.

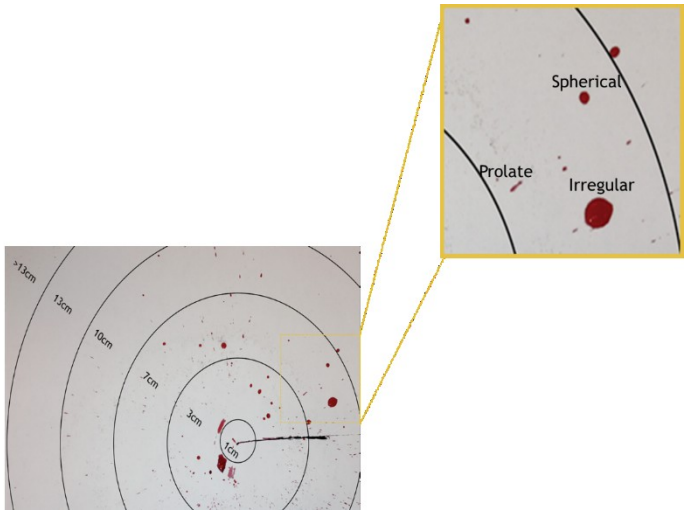

Figure 10: Bloodstain pattern created for this experiment has the different radii drawn for the purpose of catagorizing the distance at which the different types of droplets (shown in the blow up picture) impacted the paper.

Sample	Trial	Temp (°C)	C (mm^2/s)	Minutes	Seconds	Hundredths	Time (s)	Viscosity
V_1	1	22.5	0.0073557	5	13	6	313.06	2.3
	2	22.5	0.0073557	5	10	82	310.82	2.3
	3	22.5	0.0073557	5	15	2	315.02	2.3
	4	22.0	0.007356	5	23	14	323.14	2.4
	5	22.0	0.007356	5	8	93	308.93	2.3
Average								2.3
V_2	1	22.5	0.0073557	6	1	76	361.76	2.7
	2	21.0	0.0073566	6	13	33	373.33	2.7
	3	21.0	0.0073566	5	42	12	342.12	2.5
	4	21.0	0.0073566	6	15	67	375.67	2.8
	5	21.0	0.0073566	6	2	44	362.44	2.7
Average								2.7
V_3	1	20.5	0.0073569	8	10	15	490.15	3.6
	2	21.5	0.0073563	8	54	4	534.04	3.9
	3	20.0	0.0073572	7	11	81	431.81	3.2
	4	20.0	0.0073572	7	12	90	432.9	3.2
	5	20.5	0.0073569	9	8	59	548.59	4.0
Average								3.6
V_4	1	24.0	0.0073548	8	50	33	530.33	3.9
	2	24.0	0.0073548	9	55	32	595.32	4.4
	3	24.0	0.0073548	9	14	53	554.53	4.1
	4	24.0	0.0073548	9	22	31	562.31	4.1
	5	24.0	0.0073548	8	59	74	539.74	4.0
Average								4.1
V_5	1	24.0	0.0073548	10	26	59	626.59	4.6
	2	24.0	0.0073548	10	13	44	613.44	4.5
	3	24.0	0.0073548	10	56	62	656.62	4.8
	4	24.0	0.0073548	10	41	18	641.18	4.7
	5	24.0	0.0073548	10	1	31	601.31	4.4
Average								4.6

Table 3: This table is indicative of the calculations to determine the viscosities of the synthetic blood used. The material column indicates which sample was being measured. The trial column shows the trials that were conducted per viscosity. The temperature column represents the temperature of the mixture at the time of the measurement. C($\frac{mm^2}{s}$) is the callibration constant calculated by the manufactureer's instructions. The times it took for the mixture to flow throught the capillary tube are noted in the next four columns. The viscosities and average viscosities are shown in the last column

Each drop was then counted and categorized according to their radius, type, and size, then entered into Excel (Table 4). This representation table extends outward to the radius of >13cm and downward to viscosity 5 standard deviation (Appendix A).

Radius 4cm									
	Spherical			Prolate			Irregular		
Viscosity and Trial	<2mm	2-5mm	>5mm	<2mm	2-5mm	>5mm	<2mm	2-5mm	>5mm
V1T1	46	0	1	37	0	0	14	6	2
V1T2	220	4	0	21	2	0	6	5	1
V1T3	112	2	0	21	4	0	15	4	0
Average	126	2	0	26	2	0	12	5	1
Standard Deviation	88	2	1	9	2	0	5	1	1

Table 4: Categorization of the droplets, first by viscosity and trial, then by radius, shape, and size. Average and standard deviation were taken of each size.

Upon analyzing the data it was clear there were to many parameters being used to divide the data. The decision was made to eliminate the size parameter. All size counts were summed according to shape and radius. The average and standard deviation of each viscosity was calculated according to the radius and shape (Table 5).

		Spherical					Prolate					Irregular				
Viscosity	Radius (cm)	4	7	10	13	16	4	7	10	13	>13	4	7	10	13	>13
V1	Average	128	145	62	57	469	28	107	50	34	148	18	17	9	7	48
	Standard Deviation	89	78	9	7	208	7.6	73	11	16	110	5.1	4.0	3	2	18
V2	Average	85	107	94	91	633	37	115	117	58	160	25	16	10	9	46
	Standard Deviation	20	24	14	16	212	23	120	98	34	64.8	7.6	7	6	5	11
V3	Average	44	22	19	18	159	42	54	38	29	115	20	3	4	3	31
	Standard Deviation	21	8	9	7	68	19	16	6.1	5.7	27	8.5	1	3	2	3.6
V4	Average	64	41	18	35	167	15	54	35	9	18	9	8	5	1	12
	Standard Deviation	33	43	11	37	139	15	53	30	6	10	1	5	4	2	8
V5	Average	129	82	53	48	642	41	102	88	54	178	19	8	8	10	97
	Standard Deviation	53	16	26	11	394	25	5.7	31	23	110	10	7	4	5	89

Table 5: Averages and standard deviations of the viscosities according to the shape and radius.

The data was plotted on graphs (Figure 11-Figure 13) of count versus radius for each of the three shapes. The graphs show a much higher count in most of the viscosities at the greater than 13cm radius, which is labeled 16cm so the value would be accepted. This higher quantity is most likely due to the fact that there was a >3cm radius used to count the rest of the droplets. This could have been avoided by continuing to draw 3cm radii until the end of the pattern was reached. The $3.6\frac{mm^2}{s}$ and $4.1\frac{mm^2}{s}$ viscosities have lower quantities for all of the radii on all three graphs. This could possibly be a factor of not having enough trials per viscosity. It could also be the beginning of a trend that would continue, even with more numerous trials.

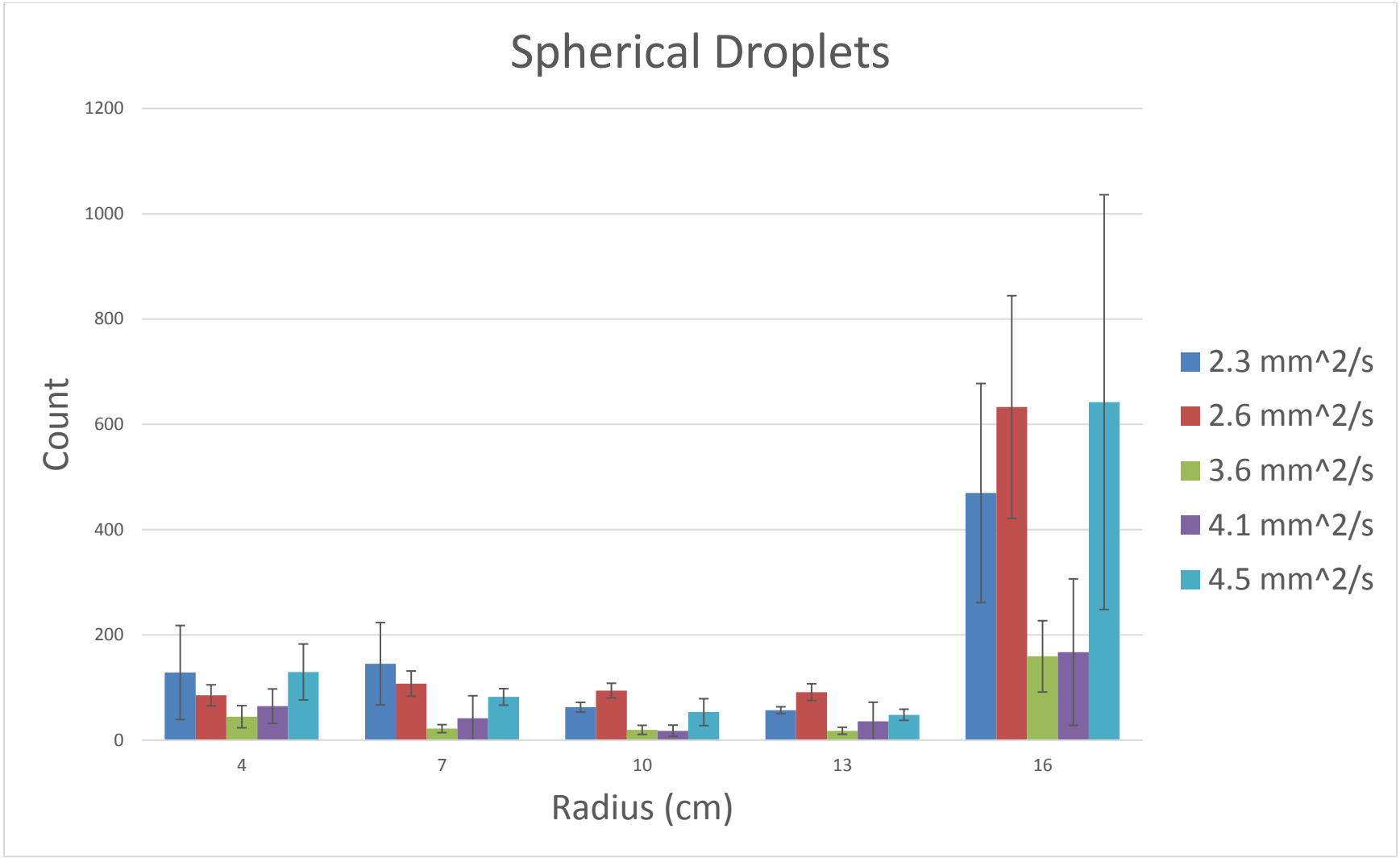

Figure 11: In this plot of count vs. radius spherical droplets were categorized into their five different viscosities and plotted according to the radius in which they impacted the paper. The colors of the bars represent the different viscosities while the error bars represent the standard deviation of each viscosity at each radius.

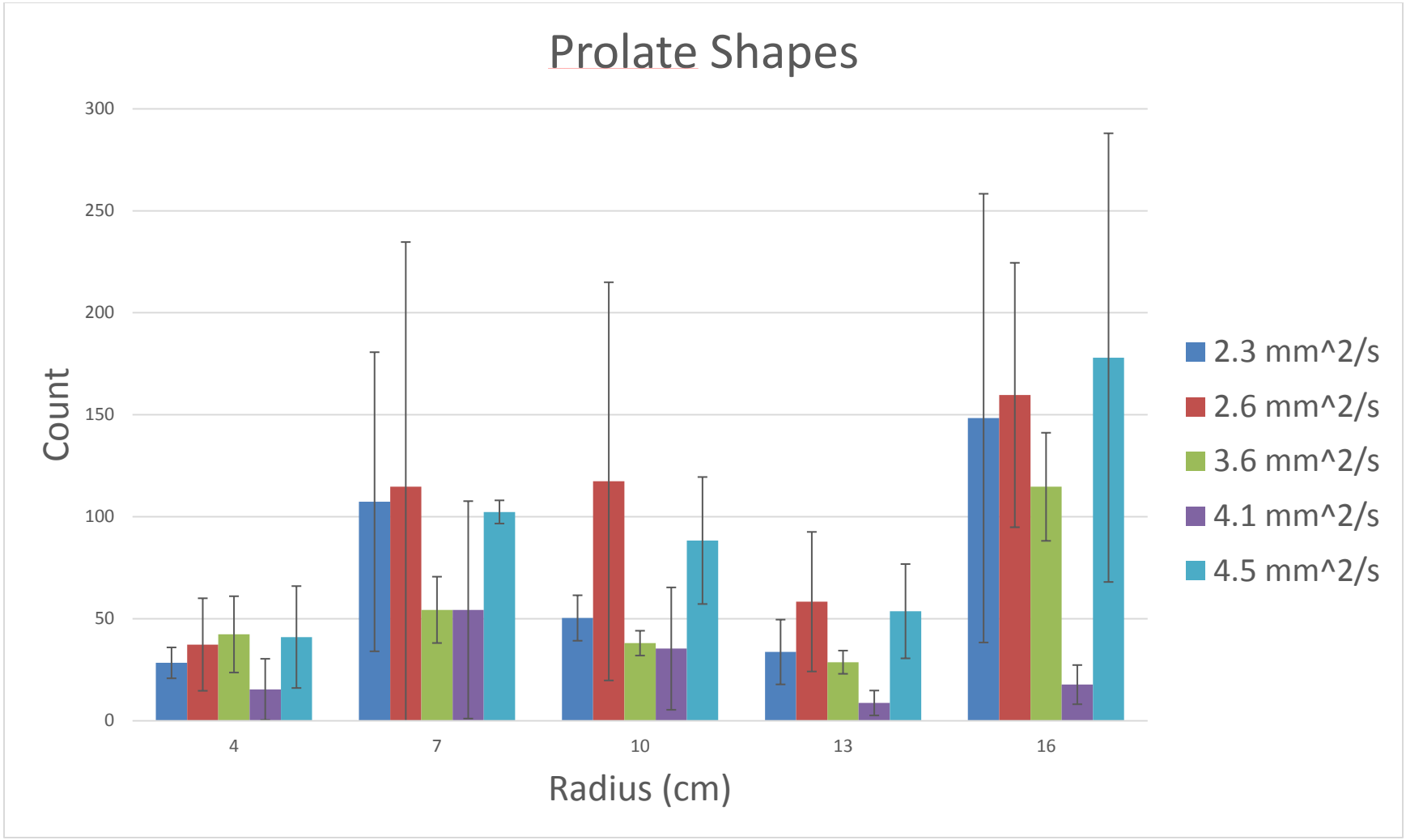

Figure 12: In this plot of count vs. radius prolate droplets were categorized into their five different viscosities and plotted according to the radius in which they impacted the paper. The colors of the bars represent the different viscosities while the error bars represent the standard deviation of each viscosity at each radius.

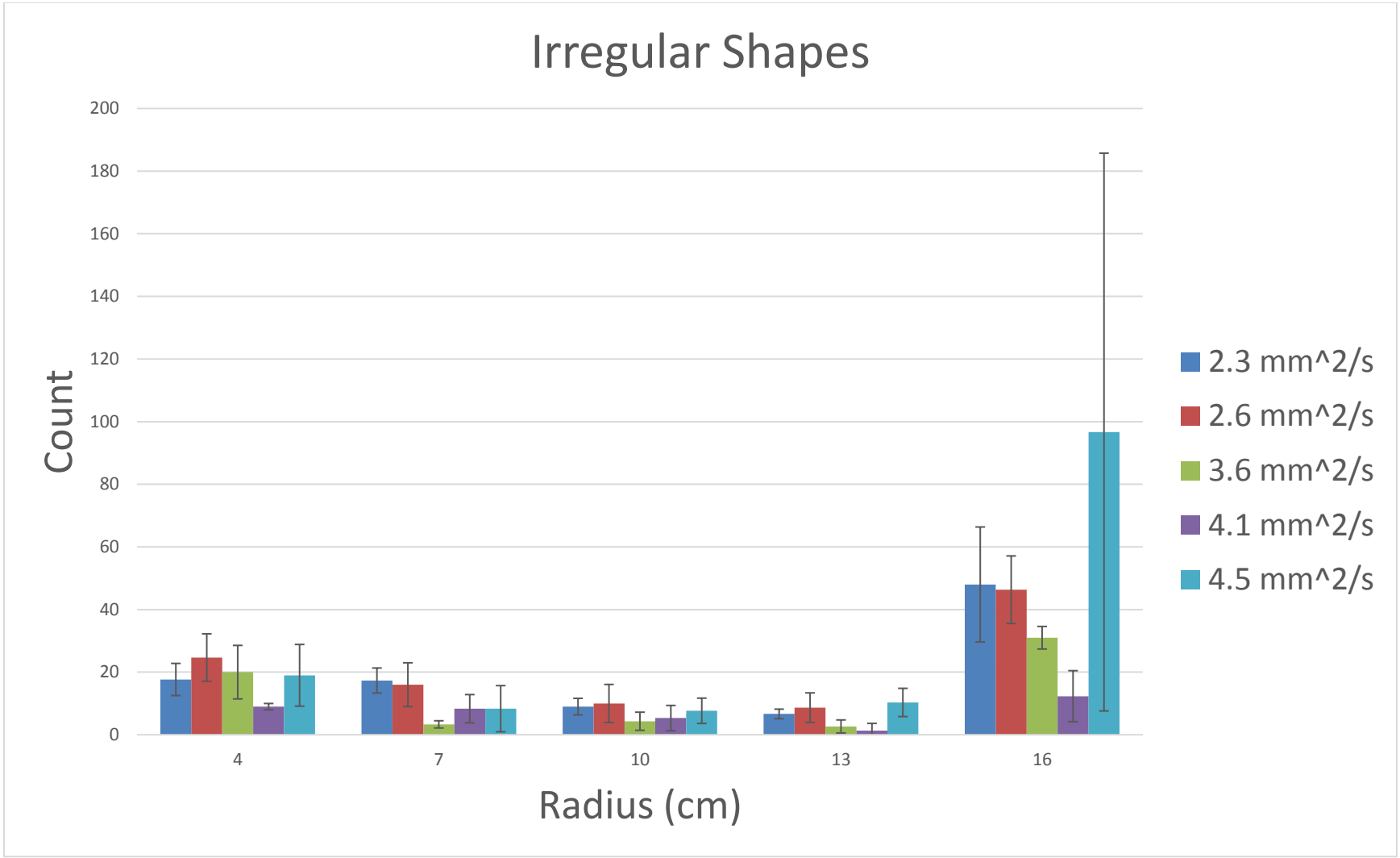

Figure 13: In this plot of count vs. radius irregular droplets were categorized into their five different viscosities and plotted according to the radius in which they impacted the paper. The colors of the bars represent the different viscosities while the error bars represent the standard deviation of each viscosity at each radius.

Each of the graphs were used to create graphs like the one here (Figure 9) useful for comparing the error bars in an attempt to differentiate between quantity of each shape according to its different viscosities. It is shown here, there is no significant difference between the viscosities because all the error bars are extremely long and overlap each other.

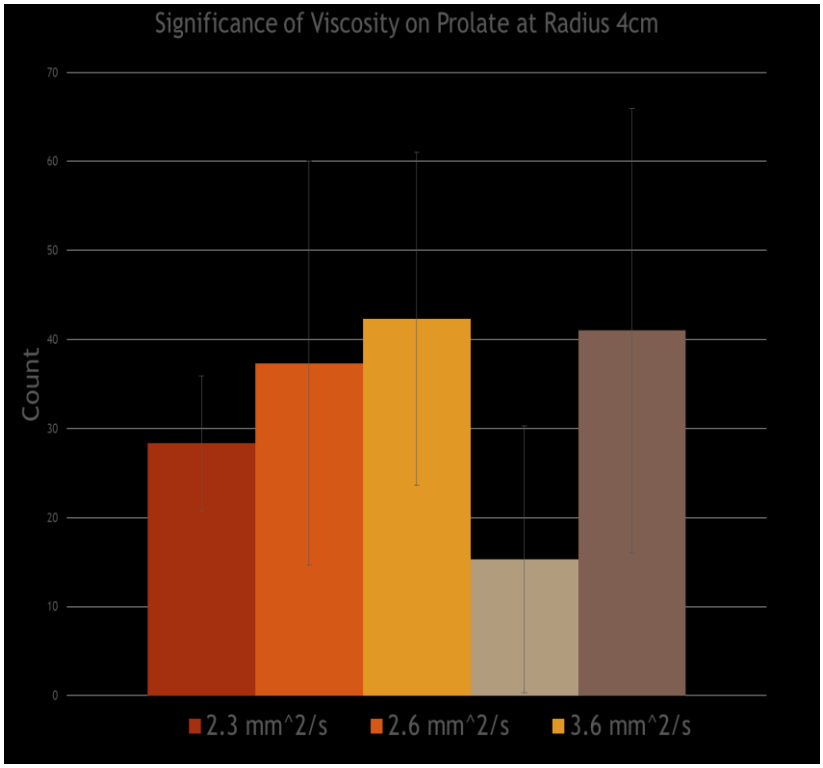

Figure 14: This figure represents the fifteen graphs plotted in count vs. viscosity for each shape at each radius. The colored bars are the different viscosities and the error bars are the standard deviation representative of the significant differences

Conclusion:

The droplet density does not appear to change in a systematic way with the viscosity. Statistical error bars due to random uncertainty is large. This does not eliminate the hypothesis that blood with lower viscosities will create more quantified, larger droplets that reach further distances, but this study shows no evidence of confirmation either.

Discussion:

Ideally, an ANOVA table should have been used to analyze the graphs, but it was apparent upon initial analysis the statistical power was not there. With this observation it was decided an ANOVA table would not be beneficial at this time.

The underlying events are replete with random uncertainties. This means it will take a very large number of trials to develop statistical significance.

Future research should include fewer viscosities and quantifiably larger trials. A suggestion is to use two viscosities; the lowest and highest humanly possible viscosities to still be living. Several more trials will be required as well because the standard deviation decreases as the number of trials increases. Thereofore, the error bars will be less likely to overlap. Once it is confirmed there is a signigicant difference, the study can then be broken down into smaller differences in viscosity in order to determine where the change takes place.

Appendix A: Raw Data

Radius 4cm									
	Spherical			Prolate			Irregular		
Viscosity and Trial	<2mm	2-5mm	>5mm	<2mm	2-5mm	>5mm	<2mm	2-5mm	>5mm
V1T1	46	0	1	37	0	0	14	6	2
V1T2	220	4	0	21	2	0	6	5	1
V1T3	112	2	0	21	4	0	15	4	0
Average	126	2	0	26	2	0	12	5	1
Standard Deviation	88	2	1	9	2	0	5	1	1
V2T1	57	4	1	26	3	0	20	5	3
V2T2	95	3	0	13	6	1	14	11	5
V2T3	90	4	1	60	3	0	7	8	1
Average	81	4	1	33	4	0	14	8	3
Standard Deviation	21	1	1	24	2	1	7	3	2
V3T1	44	1	0	46	2	0	16	1	2
V3T2	22	1	0	9	1	0	5	6	1
V3T3	61	3	1	25	5	0	22	6	1
Average	42	2	0	27	3	0	14	4	1
Standard Deviation	20	1	1	19	2	0	9	3	1
V4T1	50	3	1	6	1	0	4	3	2
V4T2	33	5	0	4	3	0	5	2	3
V4T3	93	7	1	26	6	0	2	0	6
Average	59	5	1	12	3	0	4	2	4
Standard Deviation	31	2	1	12	3	0	2	2	2
V5T1	173	2	0	59	2	0	14	2	0
V5T2	134	8	0	49	0	0	25	3	2
V5T3	70	1	0	13	0	0	6	5	0
Average	126	4	0	40	1	0	15	3	1
Standard Deviation	52	4	0	24	1	0	10	2	1

	Radius 7cm								
	Spherical			Prolate			Irregular		
Viscosity and Trial	<2mm	2-5mm	>5mm	<2mm	2-5mm	>5mm	<2mm	2-5mm	>5mm
V1T1	64	0	0	50	10	4	13	7	0
V1T2	218	2	0	46	19	1	5	7	1
V1T3	150	1	0	181	7	4	17	2	0
Average	144	1	0	92	12	3	12	5	0
Standard Deviation	77	1	0	77	6	2	6	3	1
V2T1	120	4	0	40	11	0	10	7	3
V2T2	75	5	0	39	3	0	5	3	0
V2T3	114	3	1	239	10	2	10	9	1
Average	103	4	0	106	8	1	8	6	1
Standard Deviation	24	1	1	115	4	1	3	3	2
V3T1	30	0	0	61	9	2	3	1	0
V3T2	15	0	0	33	14	4	1	2	1
V3T3	17	3	0	34	6	0	0	2	0
Average	21	1	0	43	10	2	1	2	0
Standard Deviation	8	2	0	16	4	2	2	1	1
V4T1	23	2	0	28	2	3	1	3	4
V4T2	8	1	0	9	6	0	2	1	1
V4T3	86	4	0	88	27	0	4	3	6
Average	39	2	0	42	12	1	2	2	4
Standard Deviation	41	2	0	41	13	2	2	1	3
V5T1	64	0	0	91	13	3	13	0	1
V5T2	89	1	0	89	15	0	6	0	5
V5T3	92	0	0	89	7	0	0	0	0
Average	82	0	0	90	12	1	6	0	2
Standard Deviation	15	1	0	1	4	2	7	0	3

	Radius 10cm								
	Spherical			Prolate			Irregular		
Viscosity and Trial	<2mm	2-5mm	>5mm	<2mm	2-5mm	>5mm	<2mm	2-5mm	>5mm
V1T1	57	0	0	34	6	6	6	4	0
V1T2	57	0	0	50	10	3	3	3	0
V1T3	71	2	0	22	12	8	7	2	2
Average	62	1	0	35	9	6	5	3	1
Standard Deviation	8	1	0	14	3	3	2	1	1
V2T1	93	9	1	57	5	2	11	2	0
V2T2	74	4	0	50	8	0	12	1	1
V2T3	97	4	0	197	28	5	1	2	0
Average	88	6	0	101	14	2	8	2	0
Standard Deviation	12	3	1	83	13	3	6	1	1
V3T1	21	0	0	27	12	6	3	3	0
V3T2	9	1	0	23	7	4	0	1	0
V3T3	26	1	0	20	14	1	3	3	0
Average	19	1	0	23	11	4	2	2	0
Standard Deviation	9	1	0	4	4	3	2	1	0
V4T1	29	1	0	26	10	6	1	3	6
V4T2	11	0	0	7	1	0	0	2	1
V4T3	2	10	0	42	3	11	1	1	1
Average	14	4	0	25	5	6	1	2	3
Standard Deviation	14	6	0	18	5	6	1	1	3
V5T1	75	0	0	92	29	0	9	3	0
V5T2	56	3	0	48	11	0	5	1	1
V5T3	25	0	0	73	10	2	2	2	0
Average	52	1	0	71	17	1	5	2	0
Standard Deviation	25	2	0	22	11	1	4	1	1

	Radius 13cm								
	Spherical			Prolate			Irregular		
Viscosity and Trial	<2mm	2-5mm	>5mm	<2mm	2-5mm	>5mm	<2mm	2-5mm	>5mm
V1T1	63	0	0	15	7	3	5	0	0
V1T2	50	0	0	17	5	2	2	5	1
V1T3	57	0	0	40	6	6	5	2	0
Average	57	0	0	24	6	4	4	2	0
Standard Deviation	7	0	0	14	1	2	2	3	1
V2T1	72	3	0	39	4	3	14	0	0
V2T2	81	10	0	25	7	0	7	0	0
V2T3	103	4	0	85	8	4	3	0	2
Average	85	6	0	50	6	2	8	0	1
Standard Deviation	16	4	0	31	2	2	6	0	1
V3T1	16	0	0	20	5	2	0	2	0
V3T2	12	0	0	15	6	3	1	0	0
V3T3	23	2	0	16	14	5	2	2	1
Average	17	1	0	17	8	3	1	1	0.3
Standard Deviation	6	1	0	3	5	2	1	1	0.6
V4T1	19	1	0	6	6	2	0	0	0
V4T2	6	2	1	2	0	0	1	0	3
V4T3	74	3	0	7	3	0	0	0	0
Average	33	2	0	5	3	1	0.3	0	1
Standard Deviation	36	1	1	3	3	1	0.6	0	2
V5T1	60	0	0	58	18	2	8	4	3
V5T2	38	2	0	26	4	2	5	0	5
V5T3	43	1	0	27	20	4	4	1	1
Average	47	1	0	37	14	3	6	2	3
Standard Deviation	12	1	0	18	9	1	2	2	2

	Radius >13cm								
	Spherical			Prolate			Irregular		
Viscosity and Trial	<2mm	2-5mm	>5mm	<2mm	2-5mm	>5mm	<2mm	2-5mm	>5mm
V1T1	372	20	0	79	67	21	20	19	1
V1T2	311	0	0	22	5	1	26	1	8
V1T3	697	8	0	106	105	39	31	29	9
Average	460	9	0	69	59	20	26	16	6
Standard Deviation	208	10	0	43	50	19	6	14	4
V2T1	728	12	0	85	35	16	48	3	0
V2T2	363	26	0	78	28	4	31	23	0
V2T3	725	44	0	116	95	22	19	11	4
Average	605	27	0	93	53	14	33	12	1
Standard Deviation	210	16	0	20	37	9	15	10	2
V3T1	96	4	0	40	39	17	13	11	6
V3T2	222	11	0	52	62	31	11	15	2
V3T3	141	3	0	48	41	14	17	14	4
Average	153	6	0	47	47	21	14	13	4
Standard Deviation	64	4	0	6	13	9	3	2	2
V4T1	38	36	0	5	13	10	1	2	0
V4T2	87	13	0	4	5	0	10	7	1
V4T3	221	106	0	4	12	0	4	10	2
Average	115	52	0	4	10	3	5	6	1
Standard Deviation	95	48	0	1	4	6	5	4	1
V5T1	1047	4	0	135	115	38	96	89	12
V5T2	258	6	1	32	25	4	12	14	1
V5T3	598	12	0	98	71	16	27	35	4
Average	634	7	0.3	88	70	19	45	46	6
Standard Deviation	396	4	1	52	45	17	45	39	6

[1]Tarbell KA, Brookshire JM. Evaluation of a transparent blood analog fluid Aqueous Xanthan gum/glycerin. PubMed. 1993; 107-116

[2] Centers for Disease Control and Prevention. Centers for Disease Control and Prevention, United States, 2002, 2004-2009, 2011-2012. Report

[3] Bownson DAC, Banks CE. Crime Scene Investigation: The effect of drug-contaminated bloodstains on bloodstain pattern analysis. The Royal Soc of Chem. 2010; 1885-1889

[4] James S, Kish P, Sutton T. Principles of bloodstain pattern analysis: Theory and practice. Boca Raton, FL: CRC Press; 2006. 576

[5] Ibid.

[6] Karger B, Rand S, Farcasso T, Pfeiffer H. Bloodstain pattern analysis-Casework experience Forensic Sci Intn'l. 2008; 181: 15-20

[7] Yen Y, Thali M, Kneubuehl BP, Peschel O, Zollinger U, Dirnhofer R. Blood-spatter pattern hands hold clues for the forensic reconstruction for the sequence of events. The Am Journal of For Med and Pathology. 2003; 132-140

[8] Kleibe M, Stiller D, Wiegand P. Assessment of shooting distance on the basis of bloodstain analysis and histological examinations. Forensic Sci Intn'l. 2001; 260-262

[9] Buck U, Kneubuehl B, Näther S, Albertini N, Schmidt L, Thali M. 3D bloodstain pattern analysis Ballistic reconstruction of the trajectory fo blood drops and the determination of the centres of origin of the bloodstains. Forensic Sci Intn'l. 2011; 22-28

[10] deBruin K, Stoel R, Limborgh J. Improving the point of origin determination in bloodstain pattern analysis. J Forensic Sci. 2011; 1476-1482

[11] Tarbell KA, Brookshire JM. Evaluation of a transparent blood analog fluid Aqueous Xanthan gum/glycerin. PubMed. 1993; 107-116

[12] National Council on Alcoholism and Drug Dependence http://www.ncadd.org/index.php/learn-about-alcohol/alcohol-and-crime

[13] El-Sayed M, Brownson D, Banks C. Crime scene investigation II: the effect of warfarin on bloodstain pattern analysis. Anal. Methods. 2011; 1521-1524

[14] Hamazaki T, Shishido H. Increase in blood viscosity due to alcohol drinking. PubMed. 1983; 587-594

[15] Hemospat bloodstain pattern analysis software. http://hemospat.com/bloodstain-pattern-analysis-terminology/?org=SWGSTAIN&term=impact_pattern

[16] Jung J, Lee D, Cho, Y. Non-Newtonian standard viscosity fluids. International Communications in Heat and Mass Transfer. 2013; 1-4

[17] Dictionary.com. n.d. article. 15 September 2013.

[18] Senese F. General Chemistry Online. 2010 Feb 15

[19] Peschel O, Kunz S, Rothschild M, Mützel E. Blood stain pattern analysis. Forensic Sci Med Pathol. 2011; 258-270

[20] Tice J, Lyon A, Ismagilov R. Effects of viscosity on droplet formation and mixing in microfluidic channels. Analytica Chimica Acta 2004; 73-77.